Title
Absorption of Water by the Leaves of Coast Redwood

Author
Chin, Alana

Publication Date
2021

Peer reviewed|Thesis/dissertation

Absorption of Water by the Leaves of Coast Redwood

By

ALANA CHIN

DISSERTATION

Submitted in partial satisfaction of the requirements for the degree of

DOCTOR OF PHILOSOPHY

in

Ecology

in the

OFFICE OF GRADUATE STUDIES

of the

UNIVERSITY OF CALIFORNIA

DAVIS

Approved:

Maciej Zwieniecki, Chair

Andrew McElrone

Truman Young

Committee in Charge

2021

Abstract

Like many plants, coast redwoods (*Sequoia sempervirens*), are capable of absorbing water directly into their leaves. Foliar water uptake may be important for surviving the hot, dry summers frequently found within *Sequoia's* range and influence ecosystem-level water acquisition. However the role of foliar uptake in water-stress recovery, the balance of leaf wetness and photosynthesis, and the vulnerability of foliar uptake rate to environmental perturbation are unknown. Using samples collected from throughout the crowns of tall *Sequoia* trees, this series of studies addresses these knowledge gaps and through an experimental conservation physiology approach, adds mechanistic and ecological context by incorporating a range of both high-tech and classical anatomical trait analyses. These studies together show that *Sequoia* trees can absorb up to 48 kg of water per hour across their leaf cuticles, and can use absorbed water to repair drought-damaged leaves. Foliar dimorphism allows uptake specialization in axial leaves, but wax and stomatal density cause hydraulic resistance at the leaf surface, leading to variation in uptake capabilities under different environmental conditions.

Introduction

Once considered a curious attribute of fog-adapted species, foliar water uptake is likely to occur to varying extents, in the majority of terrestrial plants (Rundel 1982, Dawson & Goldsmith 2018, Berry *et al.* 2019). Access to water beyond what is in the soil allows plants to increase productivity and perhaps recover from water stress during dry summers when leaves may become wet without soil water availability increasing (Simonin *et al.* 2009, Dawson & Goldsmith 2018). Globally, exploitation of leaf wetness makes critical contributions to plant dry-season survival and broadly influences the hydrologic cycle of vegetated ecosystems (Holder 2007, Breshears *et al.* 2008, Limm *et al.* 2009, Konrad *et al.* 2012, Eller *et al.* 2016, Emery 2016, Gotsch *et al.* 2016, Binks *et al.* 2019). However the uptake capacity of mature forest trees remains unknown. Likewise, the exact pathway by which water crosses the leaf surface is not entirely clear, water might be absorbed through the cuticle, stomata, or both (Burgess & Dawson, 2004, Kerstiens *et al.* 2006, Eller *et al.* 2013, Berry *et al.* 2019, Boanares *et al.* 2018, Guzmán-Delgado *et al.* 2021). Lack of basic knowledge in this area hampers our ability to assess variation in uptake capacity across populations and ecological gradients or detect changes in response to climatic signals.

Among the best-studied tree species, is the tallest, coast redwood, *Sequoia sempervirens* (D. Don) of the *Cupressaceae*. Existing anatomical, microclimatic, and physiological knowledge, combined with robust allometric equations for leaf area and the existence of fully crown-mapped individuals, makes *Sequoia* a model organism among forest trees (for example, Koch *et al.* 2004, Ishii *et al.* 2008, 2014, Mullin *et al.* 2009, Ambrose *et al.* 2010, 2015, Oldham *et al.* 2010, Van Pelt *et al.* 2016, Sillett & Van Pelt 2007, Kramer *et al.* 2014, Sillett *et al.* 2015, 2018, 2020, 2021). The ecological association of *Sequoia* with fog has been recognized for over a century, and its foliar water uptake ability is well documented (Cannon 1901, Cooper 1917, Azevedo & Morgan 1974, Libby 1996, Dawson 1998, Burgess & Dawson 2004, Simonen *et al.* 2008). Despite this abundant collective knowledge, we still do not know

whether fog aids redwoods in water-stress recovery, what their capacity for water absorption is, how they balance exploitation of leaf wetness with photosynthesis, how water enters their leaves, or which environmentally responsive leaf traits regulate their capacity for fog use. This dissertation seeks to tie together these long-standing loose threads in our understanding of *Sequoia's* relationship to fog and the absorption of water by its leaves.

The three Chapters of this dissertation each address open questions in the ecophysiology of *Sequoia* foliar water uptake. Chapter 1 explores how *Sequoia* leaves tolerate water stress, and establishes the role of foliar uptake in drought recovery. Following this affirmation of the importance of water absorption by leaves, Chapter 2 used samples collected from across the vertical gradient to estimate-whole tree uptake capacity and assess how foliar dimorphism helps balance the advantages and disadvantages of leaf wetness. Finally, Chapter 3 uncovers the pathway by which water crosses *Sequoia* leaf surfaces and explores the traits involved in determining uptake capacity and their environmental responsiveness. By creating a wide-ranging picture of foliar water uptake in a model species, this work attempts to establish a basis for comparison and highlights the critical importance of functional traits of leaf surfaces in determining foliar water accessibility within individual species.

Literature cited in Introduction

Azevedo, J. and Morgan, D.L., 1974. Fog precipitation in coastal California forests. Ecology, 55:1135-1141.

Berry, Z.C., Emery, N.C., Gotsch, S.G. and Goldsmith, G.R., 2019. Foliar water uptake: processes, pathways, and integration into plant water budgets. Plant, cell & environment, 42:410-423.

Binks, O., Mencuccini, M., Rowland, L., da Costa, A.C., de Carvalho, C.J.R., Bittencourt, P., Eller, C., Teodoro, G.S., Carvalho, E.J.M., Soza, A. and Ferreira, L., 2019. Foliar water uptake in Amazonian trees: Evidence and consequences. Global change biology, 25:2678-2690.

Boanares, D., Isaias, R.R.M.S., de Sousa, H.C. and Kozovits, A.R., 2018. Strategies of leaf water uptake based on anatomical traits. Plant Biology, 20:848-856.

Burgess, S.S.O. and Dawson, T.E., 2004. The contribution of fog to the water relations of Sequoia sempervirens (D. Don): foliar uptake and prevention of dehydration. Plant, Cell & Environment, 27:1023-1034.

Cannon, W.A., 1901. On the relation of redwoods and fog to the general precipitation in the redwood belt of California. Torreya, 1:137-139.

Cooper, W.S., 1917. Redwoods, rainfall and fog. The Plant World, 20:179-189.
Dawson, T.E., 1998. Fog in the California redwood forest: ecosystem inputs and use by plants. Oecologia, 117:476-485.
Dawson, T.E. and Goldsmith, G.R., 2018. The value of wet leaves. New Phytologist, 219:1156-1169.
Eller, C.B., Lima, A.L. and Oliveira, R.S., 2013. Foliar uptake of fog water and transport belowground alleviates drought effects in the cloud forest tree species, Drimys brasiliensis (Winteraceae). New Phytologist, 199:151-162.
Eller, C.B., Lima, A.L. and Oliveira, R.S., 2016. Cloud forest trees with higher foliar water uptake capacity and anisohydric behavior are more vulnerable to drought and climate change. New Phytologist, 211:489-501.
Emery, N.C., 2016. Foliar uptake of fog in coastal California shrub species. Oecologia, 182:731-742.
Fernández, V., Sancho-Knapik, D., Guzmán, P., Peguero-Pina, J.J., Gil, L., Karabourniotis, G., Khayet, M., Fasseas, C., Heredia-Guerrero, J.A., Heredia, A. and Gil-Pelegrín, E., 2014. Wettability, polarity, and water absorption of holm oak leaves: effect of leaf side and age. Plant Physiology, 166:168-180.
Gotsch, S.G., Nadkarni, N., Darby, A., Glunk, A., Dix, M., Davidson, K. and Dawson, T.E., 2015. Life in the treetops: ecophysiological strategies of canopy epiphytes in a tropical montane cloud forest. Ecological Monographs, 85:393-412.
Guzmán-Delgado, P., Laca, E. and Zwieniecki, M.A., 2021. Unraveling foliar water uptake pathways: the contribution of stomata and the cuticle. Plant, Cell & Environment.
Holder, C.D., 2007. Leaf water repellency of species in Guatemala and Colorado (USA) and its significance to forest hydrology studies. Journal of Hydrology, 336:147-154
Kerstiens, G., 2006. Water transport in plant cuticles: an update. Journal of experimental botany, 57:2493-2499.
Konrad, W., Ebner, M., Traiser, C. and Roth-Nebelsick, A., 2012. Leaf surface wettability and implications for drop shedding and evaporation from forest canopies. Pure and Applied Geophysics, 169:835-845.
Libby, W.J., 1996, June. Ecology and management of coast redwood. In Proceedings of the Conference on Coastal Redwood Ecology and Management. Humboldt State University, University of California Cooperative Extension Forestry Publication (pp. 1-4).
Limm, E.B., Simonin, K.A., Bothman, A.G. and Dawson, T.E., 2009. Foliar water uptake: a common water acquisition strategy for plants of the redwood forest. Oecologia, 161:449-459.
Rundel, P.W., 1982. Water uptake by organs other than roots. In Physiological plant ecology II (pp. 111-134). Springer, Berlin, Heidelberg.
Schreel, J.D. and Steppe, K., 2020. Foliar water uptake in trees: negligible or necessary?. Trends in Plant Science.
Simonin, K.A., Santiago, L.S. and Dawson, T.E., 2009. Fog interception by Sequoia sempervirens (D. Don) crowns decouples physiology from soil water deficit. Plant, Cell & Environment, 32:882-892.

Chapter 1

Collapsible cells and aerial water – coordination of leaf structure and function protects redwood crowns from rapid microclimatic changes

The deep crowns of tall redwoods (*Sequoia sempervirens* (D.Don) Endl.) can support > 80 vertical m of continuous foliage, reaching from shady depths with < 10 % light availability to emerge above the canopy in open sky (Sillett & Van Pelt, 2007; Oldham *et al*., 2010). Treetop leaves grow under consistently bright conditions, but little is known about the extent of microclimatic variability in the rest of the crown. Sunflecks, shafts of direct light that deeply penetrate the canopy, are capable of raising leaf temperatures by as much as 20°C in one minute (Schymanski *et al*. 2013). Such a temperature fluctuation can raise the vapor pressure deficit by ~ 2 kPa, increasing transpirational demand (ΔE). The hydraulic supply needed to sustain ΔE during sunfleck arrival potentially generates excessive tension, inducing damage to the hydraulic path within leaves if stomatal conductance (g_s) does not decrease. The time required to close stomata is not insignificant. For example, in the closely related *Metasequoia glyptostroboides* (Hu and W.C. Cheng)*,* stomatal stabilization requires ~400 seconds following a +2 kPa vapor pressure deficit increase (ΔVPD), a value consistent with other conifers (McAdam & Brodribb 2014; Martins *et al.* 2016). Relatively slow stomatal response puts leaves at risk for a sudden increase in hydraulic tension if sunflecks are not met with locally available water reserves sufficient to cover ΔE while stomata close to an aperture that will allow the leaf to survive at the new VPD level. Insufficient local hydraulic reserves might endanger key structures if tension, translated down the hydraulic path, causes embolism in woody xylem.

Conifer leaves can lose 5-20 % of their water content before losing turgor, possibly because they possess a relatively high-capacity mid-vein consisting mostly of water-filled tracheid cells (Esau 1977; Bannister 1986). Under water stress, groups of tracheids flanking the xylem, collectively called transfusion tissue (Esau 1977; Fig. 1a), can buckle (Parker 1952; Brodribb & Holbrook 2005; Zhang *et al*.

2014; Azuma *et al.* 2016), decreasing their volume. Transfusion tracheid buckling may provide water that can be used to sustain a sudden increase in evaporative demand, until stomata close, perhaps explaining why transfusion tissue volume increases with height in multiple species (Oldham *et al*. 2010; Azuma *et al.* 2016; Chin & Sillett 2019). However, transfusion tissue buckling can be followed by cavitation and formation of embolisms (Tyree & Sperry 1989), and if not refilled, buckling-based hydraulic protection would work only once. Some embolism refilling has been observed in a wide variety of plants (Holbrook *et al.* 2001; Brodersen *et al.* 2010; Johnson *et al*. 2012; Earles *et al*. 2016). In trees, embolism repair was always associated with relief of tension to values above -0.3 MPa (Secchi & Zwieniecki 2012), theoretically precluding recovery of treetop transfusion tracheids if all water comes from the soil (Brodersen & McElrone 2013) but contradicting *in situ* observations of diel changes in embolism frequency for conifers > 60 m tall (Woodruff *et al*. 2007; Johnson *et al*. 2012). Like most trees, *Sequoia* is capable of absorbing water across the surface of its leaves, possibly explaining how accumulated embolisms are repaired (Burgess & Dawson 2004; Brodersen & McElrone 2013; Schreel & Steppe 2020). Does tracheid buckling protect leaves and can foliar water uptake enable them to recover?

Our objectives are to analyze the impacts of water stress on *Sequoia* leaves, assess leaf tracheid buckling, and examine the role of foliar water uptake in stress recovery by exposing experimentally droughted leaves to dense fog. We hypothesize that transfusion tissue buckling releases a quantity of water that provides adequate temporal reserves to account for typical time delay in stomatal closure in redwood. Furthermore, foliar absorption of water may reduce xylem stress in tall conifers, permitting the refilling of collapsed and air-filled tracheids needed for cyclic protection by transfusion tissue buckling during multi-year leaf lifespans. We visualize the impacts of experimental drought and leaf wetting with synchrotron-based X-ray microtomography and explore the structural, physiological, and ecological context of our experimental results to assess the impact of cellular buckling across the full

range of potential physiological and environmental conditions. Physiological, anatomical, and climatic investigations spanning the height-gradient reveal the ways in which leaves respond to environmental signals and are thus crucial to understanding how trees function in a variable environment.

Materials and Methods

Experimental drought and exposure to fog—To extend the applicability of our results across the geographic range of *Sequoia*, we collected 10 small branches (~1 cm wood diameter) from five trees in four locations. One sample was collected at 2 m from a 18-m-tall tree on the UC Davis campus, two samples were collected from a 97-m-tall tree in Richardson Redwood Reserve, a fourth sample was collected from a 98-m-tall tree in Jedediah Smith Redwoods State Park, and six samples were collected from 101- and 103-m-tall trees at Hendy Woods State Park (all in California). The nine tall-tree sample heights ranged from 37-90 m above ground. All branches were recut under water and allowed to rehydrate through their cut stem ends for at least 48 hours (hydrated control class, N = 10, all water potentials ≥ -0.01 MPa) before sub-sampling for experimental treatments. A sub-sample was then carefully removed from each branch by cutting in melted paraffin to form a seal over the exposed surfaces (Chin & Sillett 2016). The sealed sub-sample branches were then bench dried to just before their estimated turgor loss points (Ishii *et al*., 2014), a water potential (Ψ) range of -1.9 to -2.1 MPa (droughted class, N = 10). We carefully monitored the Ψ decrease during dry-down by periodically removing individual leafy shoots from each branch and measuring their balancing pressure with a pressure chamber. Upon reaching the target Ψ, droughted branches were placed in sealed, dark plastic bags containing small pieces of wet tissue paper (not contacting the sample) and refrigerated (~ 4 °C) to prevent further water loss. Finally, a third sub-sample of branches was removed from half of the droughted branches, sealed with paraffin as above, exposed to a 7-hour fogging event (following the method in Guzmán-Delgado *et al*. 2018), and then placed in a sealed bag for 18-26 hours (fogged class,

N = 5, all Ψ ≥ -0.01 MPa). The intention of this latter approach was to mimic natural conditions where leaves were exposed to moisture and then remained wet for an extended period of time.

We selected 1 or 2 leaves from each of the 10 branches in the hydrated, droughted, and fogged treatment classes, (a total of 37 leaves, with 4 pairs of replicated leaves per treatment, N = 10 hydrated, 10 droughted, 5 fogged samples) for synchrotron-based high-resolution X-ray computed tomography (microCT) scans at the Advanced Light Source (beamline 8.3.2, Lawrence Berkeley National Labs). Leaves were detached from the shoot and placed in a pipette tip into which we breathed moist air before sealing with Parafilm to prevent further water loss. Leaves were scanned one time only (Petruzzellis *et al*. 2018) at 10X magnification for approximately 10 minutes to cover one 2-mm-long section of the mid-leaf vasculature, using scan settings and lenses optimized for plant material (Earles *et al*. 2016). MicroCT scans were analyzed using ImageJ to locate and count embolized cells over the entire 2-mm-long scanned leaf section. We quantified transfusion tracheid collapse by comparing transfusion tissue area of each experimental class using the mean of 3-8 clear cross-sectional slices per leaf scan, considering the hydrated class as our control representing pre-drought conditions. The transfusion tissue was distinguishable from mesophyll because the greater relative density of their cell walls made them appear brighter than surrounding living cells. We quantified transfusion tracheid collapse by comparing the transfusion tissue areas of the hydrated leaves to those of the droughted leaves. Volumes of water released during tracheid buckling were computed by subtracting the transfusion tissue volume of the droughted class from that of the hydrated class. The differences in transfusion tissue cross-sectional area between hydrated and droughted classes and hydrated and fogged classes were evaluated with one-sided Wilcoxon signed-rank exact tests.

Calculation of increased transpiration (ΔE) sustained by transfusion tracheid buckling—Following the drought-and-recovery experiment, we scaled-up the information obtained on tracheid buckling in leaves to its tree-level significance by bringing together existing data on leaf anatomy, stomatal conductance,

and microclimate of five tall (>109 m) individual *Sequoia* trees growing in Humboldt Redwoods State Park (hereafter HRSP-5 trees). To estimate the number of seconds of increased transpiration that could be sustained by water released during tracheid buckling, we combined the experimentally determined transfusion tissue buckling fraction (this study) with analyses of previously collected data from the HRSP-5 trees along with another set of micro-meteorological data from six additional *Sequoia* trees (Sillett & Van Pelt 2007). The HRSP-5 dataset originated from a series of companion studies (Oldham *et al*. 2010; Mullin *et al*. 2009; Ambrose *et al*. 2010), they have not been analyzed collectively before, and we use unpublished data from these studies. While it seems likely that mesophyll cells may also release water, we picture such shrinkage of living cells as being, by necessity, gradual, and in comparison to the potentially rapid buckling of non-living tracheids, a small hydraulic contribution at survivable levels.

Anatomy – We combined previously published data on transfusion tissue cross-sectional areas (from HRSP-5 trees; Oldham *et al.* 2010) with leaf length and area data for the same samples. Shoots used for this structural analysis were collected across the crown depth, from both inner and outer crown positions, in the HRSP-5 trees and fully hydrated before preservation or scanning (N = 57 samples, each of which is the mean value of 2 sectioned leaves). After verifying through additional longitudinal leaf sectioning that transfusion tissue does not taper along the length of the leaf and extends nearly to the tip (for this study), we estimated its volume by multiplying mean cross-sectional area by 95 % of total leaf length. We estimated the hydraulic capacity of transfusion tissue (mol m^{-2}) by converting volume to moles and dividing by leaf area. Potential quantities of water released by transfusion tracheid buckling in each sample were then estimated by multiplying the area-based molar quantity of water in the leaf's transfusion tissue by the buckling fraction estimated from the linear relationship between sample-height and buckling from the nine tall-tree samples. To explore other potential buckling scenarios, we also multiplied minimum and maximum buckling fractions by the molar quantities of water held in transfusion tissue.

Stomatal conductance—Using fully hydrated shoots collected from upper, middle, and lower crowns of the HRSP-5 trees (N = 15 positions, each with two replicate cuttings), maximum stomatal conductance (g_{smax}) was estimated under idealized circumstances using light response curves from a LiCor 6400 portable photosynthesis system with a 2 x 3 cm standard leaf chamber equipped with a red-blue LED source (model 6400-02B; summary data published in Mullin *et al*., 2009). Curves were made with block temperature set to 25 °C, reference CO_2 set to 400 ppm, leaf-to-air VPD maintained between 1.4 and 2.0 kPa, and the following photosynthetically active radiation (µmol m^{-2} s^{-1}) sequence: 2000, 1600, 1200, 900, 600, 400, 300, 200, 100, 50, 25, 0. For the present study, we used the individual points summarized in height-bins in Mullin et al. (2009) to develop a linear equation for the approximation of g_{smax} from sample collection-height to envision a worst-case (max observed ΔVPD at g_{smax}) response to a sudden VPD change per anatomical sample.

Micro-meteorological measurements—Treetop solar-powered micro-meteorological stations were deployed to log temperature, relative humidity, wind speed, leaf wetness and other climatic variables every half-hour over the course of one year (N = 5 sensors, N = 21,000 measurement increments) in the HRSP-5 trees. We merged these records with corresponding data collected from upper, middle, and lower crowns in six tall *Sequoia* trees from HRSP and two other primary forests (sensor locations within crowns and some totals published in Sillett & Van Pelt 2007; N = 21 sensors, 17,255 measurement increments). We used data from all 26 sensors to calculate VPD from temperature and relative humidity (Nobel 1983) in order to understand its maximum and typical values in relation to crown position. Because we were particularly interested in rapid fluctuations in evaporative demand, we calculated the intensity of local VPD increase (ΔVPD) for each sensor as the differences between sequential VPD measurements over half-hour time increments.

Calculation of seconds of transpiration sustained—We estimated the seconds of transpiration sustained by water released during transfusion tissue buckling (temporal reserves) by first calculating the

increased transpiration rate (ΔE, mol m^{-2} s^{-1}) for a given combination of stomatal conductance (g_s) and ΔVPD, using the following equation (based on Nobel 1983):

$$\Delta E = g_s \frac{\Delta \mathrm{VPD}}{99.6},$$

where 99.6 is the barometric constant for the Bull Creek alluvial forest in Humboldt Redwoods State Park. We then calculated local temporal reserves (in seconds) by dividing estimated ΔE by the molar quantity of water released per unit leaf area during tracheid collapse (mol m^{-2}). This calculation was based on the buckling fraction estimated from sample height (buckling fraction = -96.96 x height + 111.9, R^2 = 0.45, F = 5.70, P = 0.048 – tall-tree samples only, N = 9) multiplied by area-based transfusion tissue capacity (calculated from the HRSP-5 anatomy data) as follows:

$$temporal\ reserves\ (s) = \frac{\Delta E\ (mol\ m^{-2}\ s^{-1})}{transfusion\ tissue\ capacity\ (mol\ m^{-2})\ \mathrm{x}\ buckling\ fraction}$$

Available temporal reserves throughout the crown were assessed during a "worst case event" of maximum observed treetop ΔVPD events occurring at locally estimated g_{smax} (see Fig. 1.2a). As reported above, the equations for estimating buckling fraction and g_{smax} from height were based on small datasets due to the difficulty in sample collection and limited access to microCT beamtime, and are thus limited in their predictive power. To avoid over-reliance on these trends, and better explore the full range of operational conditions under which tracheids might buckle, we calculated temporal reserves for all observed combinations of g_s and ΔVPD using our maximum values (peak g_{smax} and ΔVPD across all samples) as limits to the potential ΔE space. Height-bin averages (local means of g_{smax} and max ΔVPD) defined the "expected operational range" within the full transpirational space (see Fig. 1.2c).

Results

Experimentally droughted leaves had smaller transfusion tissue cross-sectional areas than did the fully-hydrated control leaves (one-sided Wilcoxon signed rank exact test: N = 10, V = 55, P < 0.001; Fig. 1.1b,

c). Transfusion tissue buckling fraction decreased with height (reported in Methods, Fig 1.2b – excludes sample from UCD campus), ranging from a maximum reduction in area of 71 % (at 37 m), to a minimum of 23 % (at 90 m). Assuming, as we observed, similar buckling along the leaf length, then the fractional reduction in transfusion tissue cross-sectional area (buckling fraction) is equal to the fractional decrease in its volume. Fogging restored transfusion tissue area to its pre-drought level (no remaining area difference between hydrated and fogged samples, one-sided Wilcoxon signed rank exact test: N = 5, V = 6, $P = 0.6875$). Both the water-holding capacity of transfusion tissue per unit leaf area (N = 57, $R^2 = 0.44$, $F = 41.6$, $P < 0.0001$) and maximum stomatal conductance (g_{smax}) under idealized conditions increased with height (N = 14, $R^2 = 0.35$, $F = 6.40$, $P = 0.026$). Over the half-hour increments measured, the maximum single VPD increase (ΔVPD) in any individual treetop was +0.96 kPa, while below 90 m the max ΔVPD was +1.9 kPa (Fig. 1.2d). Levels of relative humidity suggest that wet air (determined here as ≥ 90 % RH) was present during 63 % of summer hours between midnight and 06:00. Treetop leaf wetness was detected at 05:30 hours on 55 % of summer mornings and was typically maintained until ~11:30. We found a greater ΔVPD (linear height trend N = 26, $R^2 = 0.37$, $F = 14.0$, $P = 0.001$) and variability in lower and middle crowns (< 90 m, $F = 0.140$, $df_{up} = 10$, $df_{low} = 14$, $P = 0.004$, SD = 0.344, $\overline{x}$ = 1.25 kPa) than in the upper crown (SD = 0.126, $\overline{x}$ = 0.94 kPa). All maximum ΔVPD events occurred between the afternoon hours of 13:00-15:00, when leaf surfaces were dry.

The observed height-decreasing buckling scenario estimated that amount of water released per m^2 of leaf area during buckling peaks at ~ 70 m above ground, while under the crown-wide minimum and maximum buckling scenarios, released water followed patterns of transfusion tissue capacity (Fig. 1.2a, c). Within the expected operational range (bounded by local means of ΔVPD and g_{smax}), transfusion tissue buckling would sustain ΔE up to 400 s, presumably long enough for stomatal closure, under nearly all conditions. While this assumes stomata behave as predicted, the estimated volume of water released appears to be tailored to this 400 s time (Fig. 1.2c). Using the range of observed buckling fractions, and

assuming a "worst case" where the maximum observed ΔVPD events coincided with full stomatal openness (*i.e.*, at g_{smax}), we found that the minimum observed buckling fraction (23 %) would be insufficient to support ΔE at most heights, unless lower and mid-crown leaves were operating well below either maximum or reported *in situ* g_s (Ambrose *et al*. 2010; Fig. 1.2c). On the other hand, under this same worst-case, when applying the maximum observed buckling fraction (71 %) to the entire crown, we estimate potentially excessive water release with the full hydraulic demand of ΔE sustained for 500-1500 s at heights > 70 m (Fig. 1.2c).

Drought treatments produced embolisms in some transfusion and xylem tracheids. While the among the eight hydrated-class leaves < 0.05 % all tracheids were air-filled, four of ten experimentally-droughted samples had embolisms in 1-15 % of tracheids, while the remaining six droughted samples had an embolism frequency of < 0.05 % of tracheids, as in the hydrated class. In the four samples that experienced cavitation, the outermost row of xylem was air-filled only in leaves from 37 and 51 m with patchy embolisms among transfusion tracheids. In all cases, fogging reduced embolism frequency to levels indistinguishable from the hydrated class (< 0.05 % tracheids were embolized, Fig. 1.3, N = 4, one-sided Fisher's exact $P = 0.014$).

Discussion

The depth of tall *Sequoia* crowns creates steep gradients in light, temperature, and relative humidity with microclimates ranging from relatively stable at the treetop to highly variable in the mid-crown. Structural and physiological plasticity of *Sequoia* leaves appears to support leaf longevity in the face of regular environmental perturbations such as the arrival of sunflecks. We observed transfusion tissue buckling under water stress in close synchronization with environmental variability, our calculations predict that tracheid buckling nearly always protects leaves within their expected operational range throughout the crown (Fig. 1.2b, c). In comparison to fully hydrated leaves, tracheid buckling induced by our experimental droughting reduces the transfusion tissue cross-sectional area by 23-71 % (X-ray

microCT images of droughted samples; Fig. 1.1b, c) with the fraction of buckling transfusion tissue decreasing with height in the crown (Fig. 1.2b). A height-associated decrease in buckling contrasts with results from *Cryptomeria japonica*, where tracheid buckling increases with height (Azuma *et al.* 2016). Deeper crowns of much taller *Sequoia* may require a balance between buckling and transfusion tissue area that supports more intense microclimatic variation in their shady depths. Compared to consistently bright treetops, we observed nearly double the intensity of ΔVPD in lower and mid-crown environments (< 90 m). There is also greater local variability in ΔVPD below 90 m with the highest intensity and broadest variation ΔVPD events occurring at 70 m, where transfusion tissue capacity is also most variable (Fig. 1.2a-e). Under our experimental conditions, foliar absorption of water fully restores transfusion tissue to its pre-drought level volume (Fig. 1.1c). Sensors detected sustained leaf-wetness events in tall *Sequoia* crowns on the majority of summer mornings, suggesting that leaves have regular access to aerial water sources. Tracheid buckling may provide protection from rising tension by halting its increase in proximal tissues at the buckling threshold, representing a stop-point for tension that isolates risk in the leaf hydraulic segment (Zhang *et al*. 2016). We picture this stop-point as the level of tension that induces enough hydraulic separation of leaf and shoot, whether through tracheid buckling or cavitation, to protect the shoot should tension continue to rise in the leaf. Such a stop-point is especially important where, as we observed in *Sequoia*, the buckling threshold is below the level of tension that results in widespread cavitation of water transport tissue.

Foliar absorption of water can restore *Sequoia* leaves to pre-drought conditions by allowing buckled tracheids to return to their previous shapes. However, under prolonged and severe drought transfusion tissue buckling does not preclude embolism, as seen here, and buckling likely decreases hydraulic conductivity (Zhang *et al*. 2014When embolisms occur after stomatal-closure they can isolate the stem from hydraulic risk (Creek *et al*. 2020; Johnson *et al*. 2012; Bouche *et al*. 2016), we imagine that cavitation could provide a secondary stopping point for tensions that exceed the buckling threshold

we observed, adding to the protective effect of buckling. Fortunately for trees with long-lived leaves, embolism occurrence may not be permanent. Water crossing the surfaces of *Sequoia* leaves is capable of refilling cavitated tracheids after reducing tension in our severed samples (Fig. 1.3). It seems reasonable that this process can occur under natural conditions, pre-dawn Ψ exceeding the gravitational potential gradient have been observed following leaf wetting in both tall *Sequoia* and *Picea sitchensis* (Jennings 2002; Kerhoulas *et al.* 2020) and sap-flow reversal has been seen in *Sequoia* (Burgess & Dawson 2004). Even if high tension due to height is permanent at the trunk, local hydraulic segmentation due to resistance between leaf and stem, or at other junctures (Zimmermann 1978; Tyree 1988; Johnson *et al.* 2016), might permit refilling at the leaf-level (Fig. 1.4). In addition to typical levels of hydraulic segmentation (Zimmermann 1978), the buckling of tracheids, and especially their cavitation, should disrupt hydraulic conductivity between leaf and stem (Bucci *et al.* 2003; Zhang *et al.* 2014). Pending repair of these impediments to flow, we envision high resistance causing an accumulation of water in the leaf, allowing local water potential to increase until the recovery threshold is met and passage into the stem can resume (Fig. 1.4). By slowing to water export from the leaf, transfusion tissue buckling may promote localized Ψ increases that facilitate embolism repair in tall trees (Fig. 1.4). The theoretical process of refilling is based on the assumption of compartmentalization of trachea or tracheid groups (Zwieniecki & Holbrook 2000) and high mesophyll hydraulic resistance that forces water to travel toward the vein. Water absorbed into living cells adjacent to the vasculature could allow embolism refilling in the manner proposed by Secchi & Zwieniecki (2010, 2012). In other conifers, such as Douglas-fir (*Pseudotsuga menziesii*), regular cycles of leaf-level embolism and repair appear to be part of their hydraulic strategy (Woodruff *et al*. 2007; Johnson *et al*. 2012). Douglas-fir may be a good candidate for recovery via foliar water absorption because ~40 % of its leaf surface area is covered in algae, presumably enhancing leaf wetness (Chin & Sillett 2019).

Presence of regular buckling cycles, and potential for embolism removal, could provide insight into *Sequoia* leaf longevity. It appears that damage accumulation is sufficiently low to allow a multi-year leaf lifespan, although both buckling and embolism fatigue warrant further investigation. Regular and sustained summertime leaf wetness, as during summer 2008 when our climate sensors were in place, may allow tall *Sequoias* to rely on transfusion tissue to repeatedly provide a hydraulic buffer against rapid fluctuations in microclimate. Maximum variability in transfusion tissue investment and peak seconds of ΔE sustained occur at ~ 70 m (Fig. 1.2a, c, e). At and below this mid-crown zone, the morphology of *Sequoia* shoots is related to light availability, but this light acclimation disappears above 70 m, although light availability rapidly increases (Ishii *et al.* 2008). The mid-crown, is the zone with both maximum intensity and variability ΔVPD and peak concentration of complex canopy structures, such as trunk reiterations. (Sillett & Van Pelt 2007; Fig. 1.2d, e). Complex mid-crown structures and high leaf area may create patchy light environments that increase the local variability brought on by sunflecks (Fig. 1.2f), contributing to local inconsistency in requirements for transfusion tissue capacity.

Does tracheid buckling provide adequate water supply to allow time for stomatal closure? While we are unlikely to have uncovered the full range of minimum and maximum buckling fractions within *Sequoia* crowns, water release under a scenario of crown-wide minimum buckling would not adequately protect the lower two-thirds of the tree (Fig. 1.2c). However, if the maximum buckling fraction is applied to the entire crown, treetops could release 8-times more water than required to allow stomatal closure (Fig. 1.2c). Our measurements suggest the height-decreasing buckling fraction we observe is optimal and can, under most combinations of g_s and ΔVPD, sustain ΔE for a minimum of 400 s, which is the approximate time reserve necessary for stomatal closure (McAdam & Brodribb 2014; Martins *et al*. 2016; Fig. 1.2c). Although behavior of stomata during our experiment and within-crown variation in closure rates in *Sequoia* are unknown, we find the closeness of our estimated values to this 400 s time to be striking, and suggestive of close coordination of hydraulic risk and transfusion tissue buckling (Fig. 1.2c). When

approaching g_{smax}, leaves may be insufficiently protected by transfusion tissue buckling when maximum levels of ΔVPD are experienced due to the sudden temperature changes brought on by sunflecks (Schymanski *et al*. 2013; Fig 1.2a, c, f). However, this "worst case" is very unlikely to be realized, because extreme ΔVPD events occur during summertime afternoons, when g_s is far below its maximum (Ambrose *et al*. 2010). In the same ~110-m-tall individual trees, *in situ* measurement of sapflow suggest that mean summertime g_s in the treetops was roughly one quarter of mean g_{smax} (~ 0.023 mol m^{-2} s^{-1} in summer; Ambrose *et al*. 2010). The area-based capacity of transfusion tissue is greatest at ~ 90 m, and estimated temporal reserves for treetop samples (108-112 m) decrease from peak mid-crown values and coalesce to a strikingly consistent range (Fig. 1.2a). This treetop consistency in temporal reserves is driven by the loss of among-tree variability in transfusion tissue capacity, perhaps suggesting that structural limits are being approached (Fig. 1.2a, e). Indeed, trees in *Sequoia's* Northern and Southernmost ranges reach similar levels of maximum transfusion tissue area at different heights, a possible explanation for why southern trees obtain heights of only ~ 80-m, where they have similar foliar hydraulic capacity to 110-m tall Northern trees (Ishii *et al.* 2014). Treetop leaves of *Sequoia* may not require as much capability to release water as elsewhere in the crown, because they exist in the least variable environment (Fig. 1.2d), are closely appressed to succulent shoots, and have smaller stomata that may be capable of faster closure (Drake *et al*. 2013; Ishii *et al*. 2014; Chin & Sillett 2019). Treetop leaves also have the widest variability in transfusion tracheid diameter and circularity (Oldham *et al*., 2010), raising the possibility of a series of buckling thresholds at greater tensions than we induced. Our analyses necessitate further consideration of the limits to maximum tree height, which include hydraulic limitation and phloem transport capacity (Ryan & Yoder 1997; Koch *et al*. 2004; Jensen & Zwieniecki 2013). Among the requirements for heights > 30 m − trees presumably too tall to refill embolisms from root-sourced water − may be adequate foliar absorption capability, and an abiotic dimension, related to presence of water on leaf surfaces. Although recovery due to foliar absorption is

crown-wide, transfusion tissue investment and physical ability to buckle could be approaching their limits in the tops of the tallest *Sequoias* (Fig. 1.2a, b). A release-refill strategy may become untenable in trees much taller than those examined here, where treetop variability in transfusion tissue capacity already becomes tightly constrained (Fig. 1.2e). The fraction of transfusion tissue that releases water may be limited by inflexibility of the extremely dense mesophyll seen at the tops of tall redwoods (Mullin *et al*. 2009; Oldham *et al*. 2010). This potential structural limitation to buckling fraction may force the prioritization of transfusion tissue at the expense of photosynthetic cells. With their pattern of investment in transfusion tissue, *Sequoias* have an almost perfectly optimized temporal reserve system to protect leaves within their expected operational ranges (Fig. 1.2c). The deep crowns of tall redwoods are supported by this finely tuned coupling of leaf vascular anatomy and stomatal conductance with microclimatic variability – a strategy that may hinge on foliar water absorption.

Chapter 1 Figures and Captions

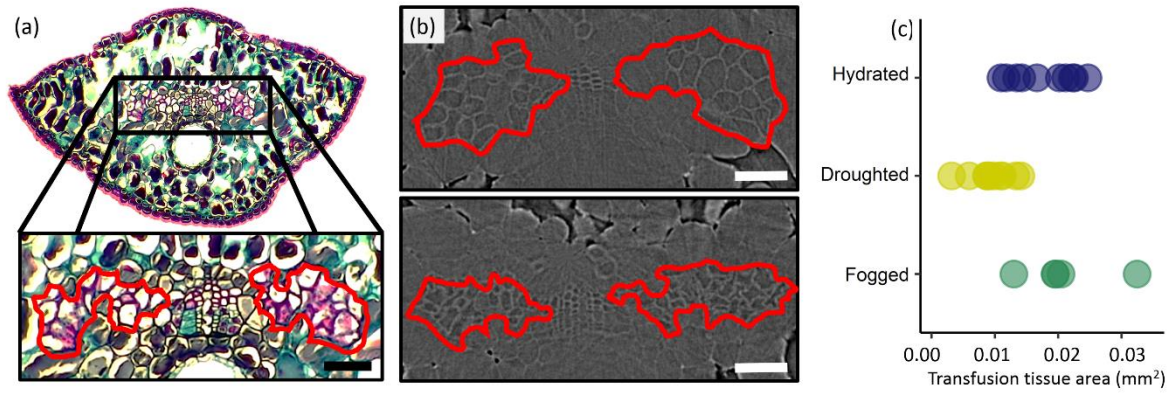

Figure 1.1. **Transfusion tissue structure and buckling. a**) The water-filled transfusion tissue (TT) of redwood leaves, outlined here in red, appears on either side of the vascular bundle in a representative leaf from 90 m. **b**) MicroCT scans of 90-m-high leaves: top panel shows round tracheids in TT of fully hydrated leaf, and bottom panel shows buckled tracheids in the TT of an experimentally droughted leaf from the same sample. Leaves scanned at 10X. **c**) TT area in hydrated (N = 10), droughted (N = 10), and fogged (N = 5) leaves. Scale bars = 0.05 mm.

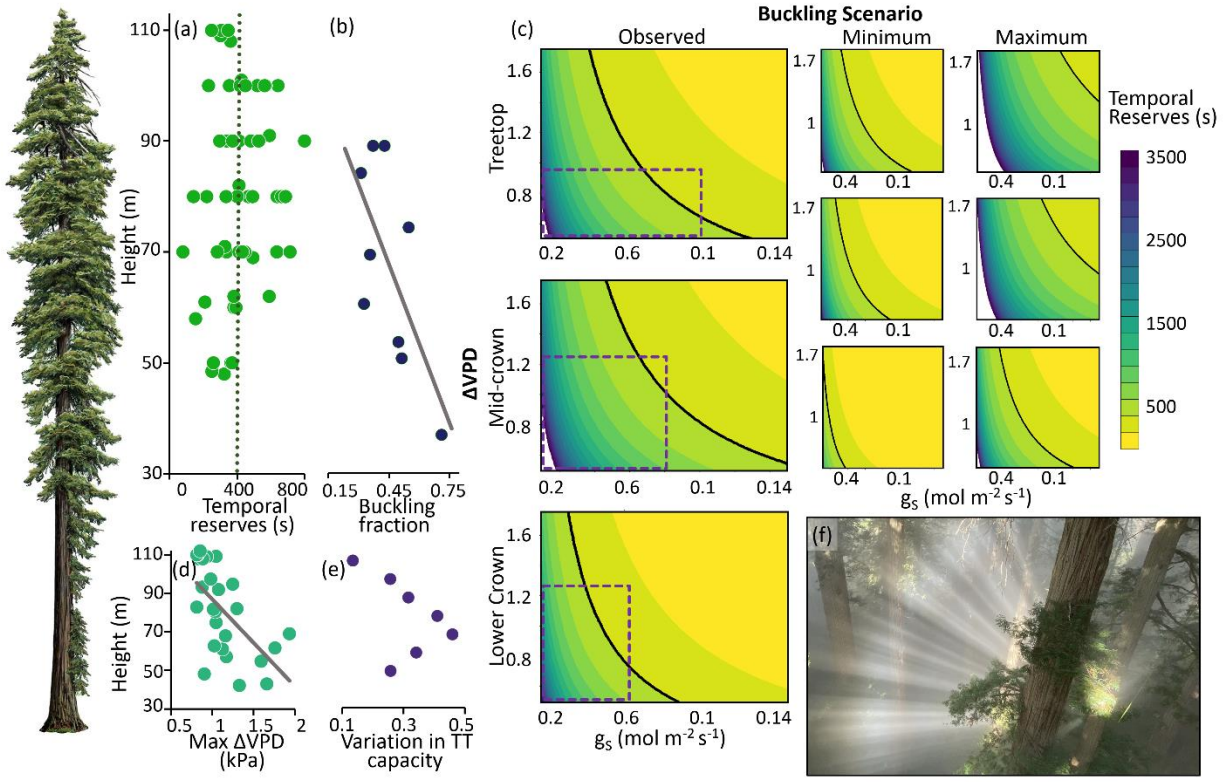

Figure 1.2. **Leaf structure and function is closely coordinated with local risk of sunflecks. a**) Number of seconds of transpiration sustained by transfusion tissue (TT) buckling, given "worst-case" where leaves operating at maximum stomatal conductance (g_{smax}) experience a maximum vapor pressure deficit increase (ΔVPD). Under the observed (height-decreasing) buckling scenario, predicted TT buckling can sustain > 400 s (green line) of worst-case ΔE for approximately half the crown with peak temporal reserves near 70 m. **b**) Fraction of the TT that buckled decreased with sample height in our drought experiment, R^2 = 0.45. **c**) Temporal reserves (seconds of ΔE sustained – color scale) provided by TT collapse are examined across the full observed ranges of ΔVPD and stomatal conductance (g_s) for observed TT buckling, as well as minimum (23 %) and maximum (71 %) buckling scenarios applied across all 3 height-bins (columns). Rows show predicted values for treetop (108-112 m), middle crown (70-90 m) and the bottom of the live crown (< 60 m) height bins. Black isolines mark the 400 s presumably needed for stomatal closure (leaves are protected by TT in the operational space to the left of these lines). Dashed purple boxes, shown only in the observed scenario, represent the expected operational range for each height bin, bounded by the local means of g_{smax} and maximum ΔVPD. **d**) Within-crown distribution of maximum VPD increases over half-hour increments reveals widely variable change and greater extremes below 80 m. **e**) Coefficients of variation (SD/mean) in TT capacity per unit leaf area in 10 m height-bins peaks at 70 m, and is lowest in the treetops, similar to peak variability in ΔVPD. **g**) Sunflecks rapidly increase light availability in the deeply-shaded lower crown. Tree illustration on left provided by Robert Van Pelt.

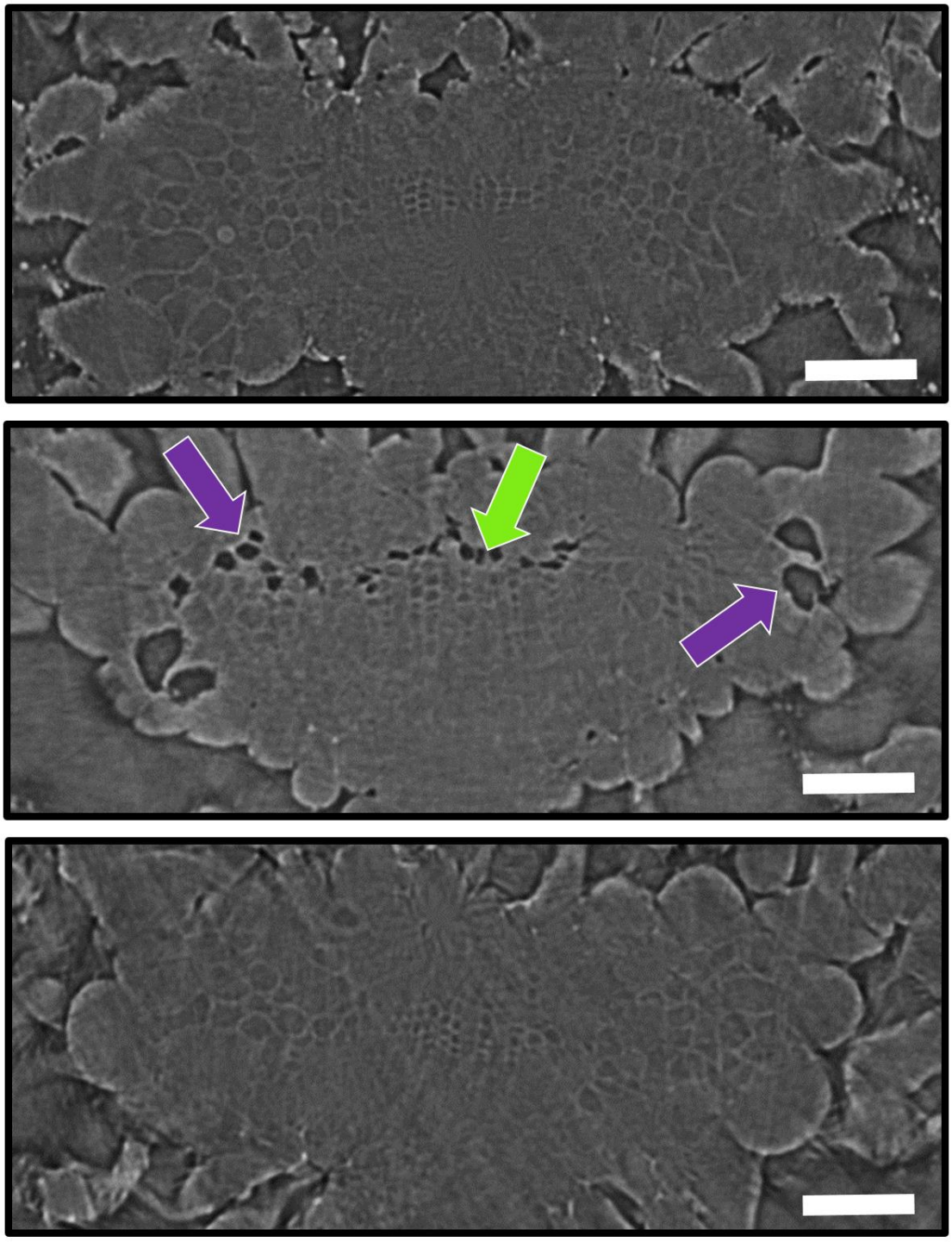

Figure 1.3. **Drought induced embolism and recovery from foliar water absorption**. Visualized with microCT scans, leaves fully rehydrated via shoot cut-ends (**a**) lack widespread embolized tracheids. Some experimentally droughted leaves (**b**) had embolized tracheids (black cells) in transfusion tissue (purple arrows) and xylem (green arrow). Following exposure to fog, all previously droughted leaves (**c**) lacked embolisms. All leaves from 51 m, scale bars = 0.05 mm.

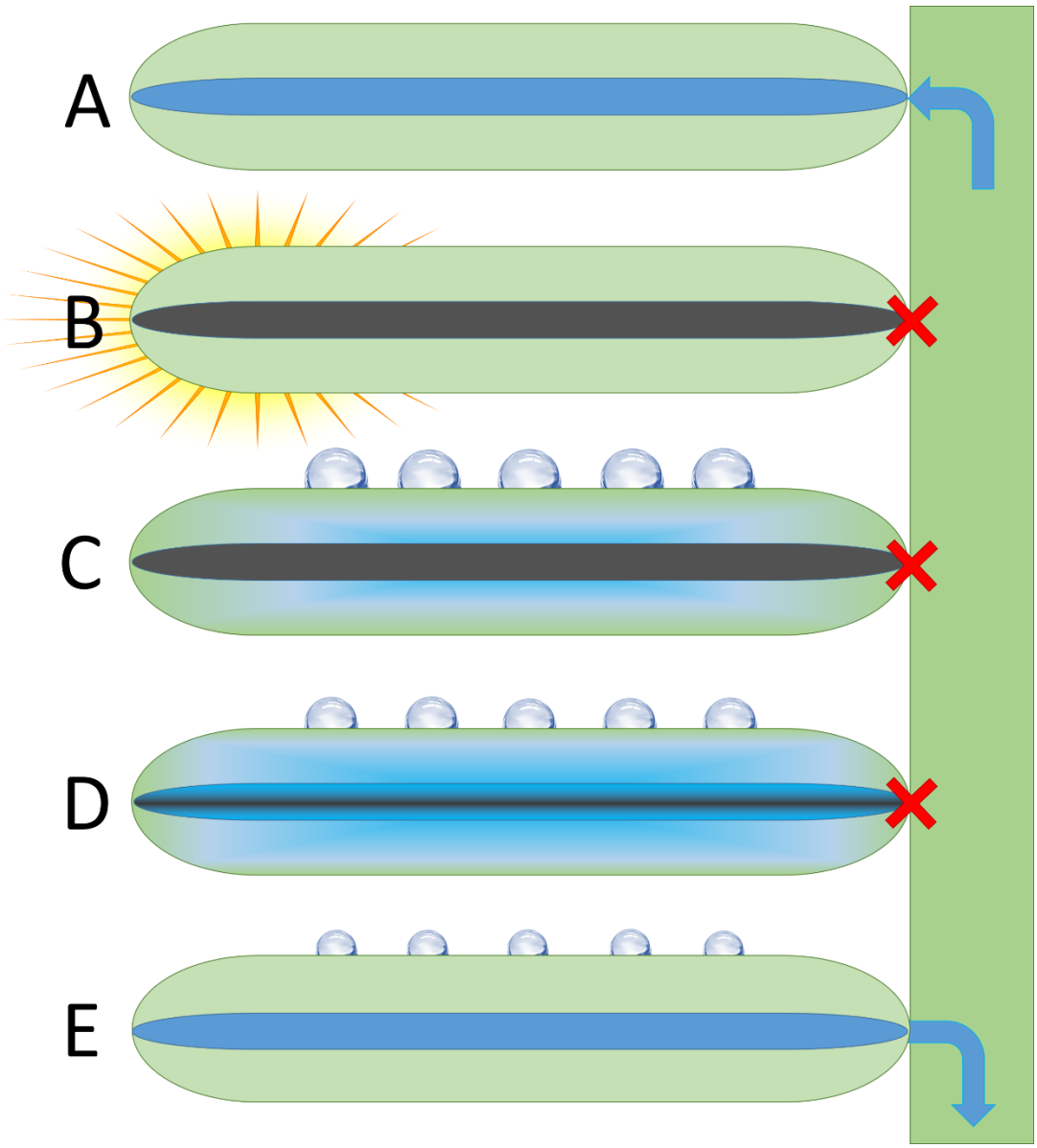

Figure 1.4. A conceptual model illustrating hydraulic-tissue repair following foliar water uptake in tall trees. A) Under typical transpirational conditions, water moves from the stem into the leaf vein. Resistance at the juncture between leaf and stem (hydraulic segmentation, Zimmermann 1978) allows the leaf to reach lower water potentials. **B)** During water-stress events, buckling and cavitation of the leaf vascular tissue restricts hydraulic conductance between leaf and stem, protecting the stem from excessive tension by partially or fully isolating it from the leaf. **C)** Subsequent leaf wetting allows water to enter the leaf, where it is retained due to disrupted vascular conductivity. Tracheid buckling may thereby facilitate the embolism repair process by increasing resistance to water export. **D)** Water potential in the leaf continues to rise until the repair threshold is met. **E)** Following the restoration of hydraulic conductivity, potential of xylem sap in the leaf equilibrates with that of the stem.

Literature Cited in Chapter 1

Ambrose, A.R., Sillett, S.C., Koch, G.W., Van Pelt, R., Antoine, M.E. and Dawson, T.E. 2010. Effects of height on treetop transpiration and stomatal conductance in coast redwood (Sequoia sempervirens). *Tree Physiol.* 30:1260-1272.

Azuma, W., Ishii, H.R., Kuroda, K. and Kuroda, K. 2016. Function and structure of leaves contributing to increasing water storage with height in the tallest Cryptomeria japonica trees of Japan. *Trees* 30:141-152.

Bannister, P. 1986. Drought resistance, water potential and water content in some New Zealand plants. *Flora* 178:23-40.

Bouche, P.S., Delzon, S., Choat, B., Badel, E., Brodribb, T.J., Burlett, R., Cochard, H., Charra-Vaskou, K., Lavigne, B., Li, S. and Mayr, S. 2016. Are needles of Pinus pinaster more vulnerable to xylem embolism than branches? New insights from X-ray computed tomography. *Plant, cell & environment* 39:860-870.

Brodersen, C. and McElrone, A. 2013. Maintenance of xylem network transport capacity: a review of embolism repair in vascular plants. *Front. Plant Sci.* 4:108.

Brodersen, C., Mcelrone, A., Choat, B., Matthews, M., and Shackel, K. 2010. The dynamics of embolism repair in xylem: in vivo visualizations using high-resolution computed tomography. *Plant Physiol.* 154:1088–1095.

Brodribb, T.J. and Holbrook, N.M. 2005. Water stress deforms tracheids peripheral to the leaf vein of a tropical conifer. *Plant Physiol.* 137:1139-1146.

Burgess, S.S.O. and Dawson, T. 2004. The contribution of fog to the water relations of Sequoia sempervirens: foliar uptake and prevention of dehydration. *Plant, cell & environment* 27:1023-1034.

Chin, A.R. and Sillett, S.C. 2016. Phenotypic plasticity of leaves enhances water-stress tolerance and promotes hydraulic conductivity in a tall conifer. *Am. J. Bot*. 103:796-807.

Chin, A.R. and Sillett, S.C. 2019. Within-crown plasticity in leaf traits among the tallest conifers. *Am. J. Bot*. 106:174-186.

Creek, D., Lamarque, L.J., Torres-Ruiz, J.M., Parise, C., Burlett, R., Tissue, D.T. and Delzon, S. 2020. Xylem embolism in leaves does not occur with open stomata: evidence from direct observations using the optical visualization technique. *J Exp. Bot.* 71:1151-1159.

Drake, P.L., Froend, R.H. and Franks, P.J. 2013. Smaller, faster stomata: scaling of stomatal size, rate of response, and stomatal conductance. *J. Exp. Bot.* 64:495-505.

Earles, J.M, Sperling, O., Silva, L.C., McElrone, A.J., Brodersen, C.R., North, M.P. and Zwieniecki, M.A. 2016. Bark water uptake promotes localized hydraulic recovery in coastal redwood crown. *P. C.& E.* 39:320-328.

Esau, K. 1977. Anatomy of seed plants. John Wiley & Sons. Inc. New York, NY.

Guzmán-Delgado, P., Earles, M.J. and Zwieniecki M.A., 2018. Insight into the physiological role of water absorption via the leaf surface from a rehydration kinetics perspective. P. C.& E. 41:1886-1894.Holbrook, N. M., Ahrens, E. T., Burns, M. J., and Zwieniecki, M. A. 2001. In vivo observation of cavitation and embolism repair using magnetic resonance imaging. Plant Physiol. 126:27–31.

Ishii, H.T., Jennings, G.M., Sillett, S.C. and Koch, G.W., 2008. Hydrostatic constraints on morphological exploitation of light in tall *Sequoia sempervirens* trees. *Oecologia*, 156:751-763.

Ishii, H.R., Azuma, W., Kuroda, K. and Sillett, S.C. 2014. Pushing the limits to tree height: could foliar water storage compensate for hydraulic constraints in *Sequoia sempervirens*? *Func. Eco*. 28:1087-1093.

Jennings, G.M. 2002. Vertical hydraulic gradients and the cause of foliar variation in tall redwood trees (*Sequoia sempervirens.*) *Masters Thesis*, Humboldt State University.

Jensen, K.H. and Zwieniecki, M.A. 2013. Physical limits to leaf size in tall trees. *Phys. Rev. Let*. 110:018104.

Johnson, D.M., Wortemann, R., McCulloh, K.A., Jordan-Meille, L., Ward, E., Warren, J.M., Palmroth, S. and Domec, J.C. 2016. A test of the hydraulic vulnerability segmentation hypothesis in angiosperm and conifer tree species. *Tree Physiol.*, 36:983-993.

Johnson, D.M., McCulloh, K.A., Woodruff, D.R. and Meinzer, F.C. 2012. Hydraulic safety margins and embolism reversal in stems and leaves: why are conifers and angiosperms so different?. *Plant Science* 195:48-53.

Kerhoulas, L.P., Weisgrau, A.S., Hoeft, E.C. and Kerhoulas, N.J., 2020. Vertical gradients in foliar physiology of tall *Picea sitchensis* trees. *Tree Physiol.* 40:321-332.

Koch, G.W., Sillett, S.C., Jennings, G.M. and Davis, S.D. 2004. The limits to tree height. *Nature* 428:851-854.

Martins, S.C., McAdam, S.A., Deans, R.M., DaMatta, F.M. and Brodribb, T.J. 2016. Stomatal dynamics are limited by leaf hydraulics in ferns and conifers: results from simultaneous measurements of liquid and vapor fluxes in leaves. *Plant, cell & environment* 39:694-705.

McAdam, S.A. and Brodribb, T.J. 2014. Separating Active and Passive Influences on Stomatal Control of Transpiration. *Plant Physiol*. 164:1578-1586.

Mullin, L.P., Sillett, S.C., Koch, G.W., Tu, K.P. and Antoine, M.E. 2009. Physiological consequences of height-related morphological variation in Sequoia sempervirens foliage. *Tree Physiol*. 29:999-1010.

Nobel, P.S. 1983. *Biophysical plant physiology and ecology*. WH Freeman and company.

Oldham, A.R., Sillett, S.C., Tomescu, A.M. and Koch, G.W. 2010. The hydrostatic gradient, not light availability, drives height-related variation in Sequoia sempervirens (Cupressaceae) leaf anatomy. *Am. J. Bot.* 97:1087-1097.

Parker, J. 1952. Desiccation in conifer leaves: anatomical changes and determination of the lethal level. *Bot. Gazette* 114:189-198.

Petruzzellis, F., Pagliarani, C., Savi, T., Losso, A., Cavalletto, S., Tromba, G., Dullin, C., Bär, A., Ganthaler, A., Miotto, A. and Mayr, S. 2018. The pitfalls of in vivo imaging techniques: evidence for cellular damage caused by synchrotron X-ray computed micro-tomography. *New Phyt*. 220:104-110.

Ryan, M.G. and Yoder, B.J. 1997. Hydraulic limits to tree height and tree growth. *Biosci.* 47:235-242.

Schreel, J.D.M, and Steppe, K. 2020. Foliar water uptake in trees: negligible or necessary? *Trends in Plant Science.*

Schymanski, S.J., Or, D. and Zwieniecki, M. 2013. Stomatal control and leaf thermal and hydraulic capacitances under rapid environmental fluctuations. *PloS one* 8:e54231.

Secchi, F. and Zwieniecki, M.A. 2012. Analysis of xylem sap from functional (nonembolized) and nonfunctional (embolized) vessels of Populus nigra: chemistry of refilling. *Plant Physiol*. 160:955-964.

Sillett, S.C. and Van Pelt, R. 2007. Trunk reiteration promotes epiphytes and water storage in an old-growth redwood forest canopy. *Eco. Mon.* 77:335-359.

Tyree, M.T. 1988. A dynamic model for water flow in a single tree: evidence that models must account for hydraulic architecture. *Tree Physiology*, 4:195-217.

Tyree, M.T. and Sperry, J.S. 1989. Vulnerability of xylem to cavitation and embolism. *Ann. Rev. Plant Bio.* 40:19-36.

Woodruff, D.R., McCulloh, K.A., Warren, J.M., Meinzer, F.C. and Lachenbruch, B. 2007. Impacts of tree height on leaf hydraulic architecture and stomatal control in Douglas-fir. *P., C, & E,* 30:559-569.

Zhang, Y.J., Rockwell, F.E., Graham, A.C., Alexander, T. and Holbrook, N.M. 2016. Reversible leaf xylem collapse: a potential “circuit breaker” against cavitation. *Plant Physiol.* 172:2261-2274.

Zhang, Y.J., Rockwell, F.E., Wheeler, J.K. and Holbrook, N.M. 2014. Reversible deformation of transfusion tracheids in Taxus baccata is associated with a reversible decrease in leaf hydraulic conductance. *Plant Physiol.* 165:1557-1565.

Zimmermann MH. 1978. Hydraulic architecture of some diffuse-porous trees. *Canadian Journal of Botany* 56: 2286–2295.

Chapter 2

Shoot dimorphism enables *Sequoia sempervirens* to separate contrasting requirements for foliar water uptake and photosynthesis

The ecological strategy of coast redwood (*Sequoia sempervirens* D. Don), a tree of California's seasonally dry temperate rainforest, is one of longevity. *Sequoia* maintains dominance in the presence of co-occurring conifers, because it outlasts them by several life-spans (Sillett *et al.* 2021). The longevity and persistent growth of *Sequoia* supports the development of a deep-canopied multi-species forest capable of attaining global maximum biomass and leaf area (Van Pelt *et al*. 2016, Sillett *et al*. 2020). In addition to massive trunks and limbs, *Sequoia'*s investments in longevity include tannin-rich heartwood, fire-resistant bark, and pest-resistant leaves (Fritz 1931, Clark & Scheffer 1983, Espinosa-García *et al.* 1991, Davies *et al.* 2014). Leaf-level phenotypic plasticity allows tall *Sequoia* to optimize traits across deep crowns in response to environmental conditions, particularly water stress (Oldham *et al.* 2010, Van Pelt *et al*. 2016, Chin & Sillett 2019). *Sequoia* exhibits distinctive heteroblastic shoot development, characterized by abrupt metamorphic transitions between thick, woody 'axial' shoots with highly decurrent scale-leaves and the initially-pliable 'peripheral' shoots they support, which comprise ~ 95 % of the total leaf area (**Fig. 2.1,** Jones 1999). This striking dimorphism is in addition to the broad, though gradual, allomorphic changes with height seen among peripheral shoots (Koch *et al.* 2004, Oldham *et al.* 2010, **Fig. 2.1**). While the capacity of redwoods to absorb water through leaves and improve tree water status is well documented (Burgess & Dawson 2004, Simonen *et al.* 2008), causes of variation in foliar uptake capacity remain untested experimentally. Specifically, analysis of within-crown variation in foliar uptake is missing, limiting our ability to identify environmentally-responsive leaf traits regulating water absorption or to investigate the consequences of whole-tree foliar uptake across the broad climatic range redwood occupies (**Table 2.1**).

Trees face trade-offs between foliar uptake and photosynthesis when leaves are wet (Smith & McClean 1989, Ishibashi & Terashima 1995, Dawson & Goldsmith 2018). Absorption of water across leaf surfaces allows trees to avoid or recover from drought-induced hydraulic damage, maintain photosynthetic rates, relieve low xylem water potentials (Ψ), and initiate turgor-driven growth (Breshears *et al.* 2008, Simonen *et al.* 2008, Eller *et al.* 2013, Emery 2016, Steppe *et al.* 2018, Chin *et al*. 2021). Foliar uptake capacity is associated with leaf surface properties (Limm & Dawson 2010, Fernández *et al.* 2014, Jura-Morawiec & Marcinkiewicz 2020). Trees, which appear to be especially reliant on foliar uptake, may have leaf-surface traits more associated with foliar uptake than other growth forms in similar environments (Neinhaus & Barthlott 1997, Schreel & Steppe 2020). However, if leaf stomata are covered by films of water, photosynthesis can be suppressed (Smith & McClean 1989, Ishibashi & Terashima 1995, Hanba *et al*. 2004, Gerlein-Safdi *et al.* 2018, Berry & Goldsmith 2020). Ability to absorb water through leaves is widespread, but its capacity may be highly variable within and among taxa and environments (Gotsch *et al.* 2015, Berry *et al.* 2018, Dawson & Goldsmith 2018, Binks *et al.* 2019). In seasonally dry forests, foliar uptake can be a key component of tree drought-survival (Yates & Hutley 1995, Schreel *et al.* 2019), whereas trees in perpetually wet forests may have evolved adaptations to avoid leaf wetness, allowing photosynthesis to proceed during long wet periods by keeping stomata dry (Field *et al.* 1998, Holder 2007a, Aparecido *et al*. 2017). In seasonal rainforests, trees that rely on foliar uptake to survive the dry season (Yates & Hutley 1995, Eller *et al.* 2013) must also cope with a prolonged and intense rainy season that might limit photosynthesis by allowing water films to cover stomata. In *Sequoia* the hydraulic benefits of foliar uptake (Burgess & Dawson 2004, Simonen *et al.* 2008, Chin *et al.* 2021) coexist with a capacity to maintain high wet-season stomatal conductance despite the nearly constant presence of aerial water (Ambrose *et al.* 2010). How does *Sequoia* balance the contrasting requirements of water absorption and water repellency to flourish in wet and dry forests? Variation in leaf interactions with water may have broad ecological implications, as

the degree to which water is shed from, absorbed into, or evaporated off leaf surfaces influences forest hydrology, precipitation dependence, and drought susceptibility (Holder 2007b, Berry *et al.* 2008, Konrad *et al.* 2012, Schreel & Steppe 2020).

Foliar uptake is driven by the Ψ gradient between the wet leaf surface and the interior of the leaf (Rundel 1982, Berry *et al.* 2008). In obedience to Ohm's Law, hydraulic flux into the leaf should be proportional to the interaction between the Ψ gradient and hydraulic resistance at the leaf surface. The gravitational component of Ψ contributes ~ -1 MPa to the hydraulic tension at the top of a 100 m tall tree, creating a natural gradient in the potential energy available to power foliar uptake in tall trees. However, foliar uptake rates do not always increase along the Ψ gradient (Limm & Dawson 2010, Schreel *et al.* 2019), indicating that resistance can dominate the system. Wide variation in foliar uptake capacity among species (Limm *et al.* 2009, Gotsch *et al.* 2015, Emery *et al.* 2016, Guzmán-Delgado *et al.* 2017, Schreel *et al.* 2019) is evidence that while the Ψ gradient may be the force driving uptake (Berry *et al.* 2018), leaf-surface features determine its maximum rate. In contrast to Ψ, variation in leaf-surface hydraulic resistance is most likely determined by a suite of factors that affect leaf absorptive capacity and can respond to the local environment given adequate plasticity. Leaf traits affecting uptake rate, which may control surface resistance, are most likely those related to surface-water interactions, stomatal density and size, structure of epicuticular waxes, and stomatal plugs (Barthlott *&* Neinhaus 1996, Field *et al.* 1998, Rosado *et al*. 2010, Aparecido *et al.* 2017, Kerhoulas *et al.* 2019). These surface traits can change with crown position (Rosado *et al*. 2010, Chin & Sillett 2019) and, in *Sequoia*, may be different between dimorphic shoot types (**Fig. 2.1**). Variability in foliar uptake capacity across shoot types leads us to hypothesize that availability of local resources (light and aerial water) may control shoot developmental plasticity, separating foliar uptake and photosynthesis.

Sequoia thrives in seasonally dry coastal rainforests as well as much drier forests farther from the ocean, where it tolerates hot, dry summers and survives infrequent but severe droughts. We explore

how foliar uptake in *Sequoia* is balanced with the primary photosynthetic function of leaves. We suspect that shoot dimorphism provides a means of optimizing carbon acquisition while maintaining shoot longevity by separation of functional leaf traits promoting either water uptake or permitting photosynthesis on wet days between. If aerial water accessibility is determined by leaf traits that change surface hydraulic resistance, then leaf structural variation will influence foliar uptake capacity independent of the Ψ gradient. To evaluate the broader significance of foliar uptake to *Sequoia* function, we make the first whole-crown estimates of water uptake capacity for any tree, using some of the largest individual trees known. We use uptake measurements from peripheral and axial shoots collected across the vertical distribution of *Sequoia* foliage, scaled-up by branch- and tree-level allometry (Kramer *et al.* 2014, Sillett *et al.* 2015, 2020), to quantify foliar uptake and reveal its potential contributions to whole-tree water balance and forest hydrology.

Methods

Measurement of leaf traits – We took a multifaceted approach to leaf trait measurements, combining traditional anatomical cross-sections, acrylic imprints, and high-resolution macro composite-imaging. Within each sample branch (also used for experimental fogging), we separated leaves on peripheral and axial shoots for purposes of trait analysis. While our emphasis was on surface traits, we also compared the vascular anatomy of peripheral and axial leaves to understand their functional roles (**Table 2.1**). We fixed fresh peripheral and axial leaves in FPA, embedded them in paraffin, and cut 10 µm cross-sections on a rotary microtome. After staining slides with methylene blue and safranin, the vascular bundle (xylem, transfusion tissue, phloem, and fibers) was photographed at 20X. To verify that the phloem structural differences were not artifacts of slide preparation, we examined additional fresh green sections of axial leaves. We prepared acrylic resin (nail polish) imprints of the adaxial and abaxial leaf surfaces and photographed them at 10X for measuring stomatal density and 40X for measuring

guard cell length. As guard cell length is strongly correlated with stomatal pore area, it serves as a reliable index for stomatal covering fraction (stomatal pore area per leaf area). Further, we measured the covering fraction of visible epicuticular waxes (wax area per leaf area) and documented the distribution of epiphyllous organisms using composites created from stacked macro-images of adaxial and abaxial leaf surfaces taken at slightly different focal depths to create seamless high-resolution surface images (**Fig. 2.2a, b**). We verified that the white substances photographed (**Figs. 2.2a, 2.3b**) were indeed epicuticular waxes by dipping leaves in chloroform, which retains (potentially white) fungi on the leaf but removes wax. We were unable to measure adaxial surface traits for axial leaves because of a heavy covering of epiphyllous organisms (**Fig. 2.2b**). All images were analyzed with Fiji ImageJ (NIH).

After observing differences in the internal anatomy of peripheral and axial leaves (**Fig. 2.2c, d**), we took the additional step of measuring photosynthesis and stomatal conductance on sets of peripheral (N = 5) and axial (N = 7) shoots reachable from ground level. We recognize that measurements of photosynthesis are related to sample collection height (Mullin *et al*. 2009), however we assume that physiological differences between axial and peripheral shoots will hold across the crown, as their structural differences remain consistent. Without detaching shoots from trees, we analyzed each with a LiCor 6400 equipped with a conifer chamber, deliberately choosing shoots in both sun and shade. We then removed the shoots, dissected them, and scanned their leaves to determine area.

Measurement of foliar uptake − We collected a total of 16 small *Sequoia* branches from 6 individual trees at 5 climatically distinct forest locations (latitude 36° to 41° N, **Tables 2.1, 2.4**) that yielded high trait diversity (**Table 2.1**). Branches were collected at heights ranging from 22 to 102 m above ground level. After collection, branches were recut under water and allowed to rehydrate completely before beginning measurements. In the lab, branch ends were recut in melted paraffin to create a seal (Chin & Sillett 2016) and bench-dried until within ± 0.03 MPa of the estimated pre-dawn

maximum Ψ for their collection height based on the gravitational potential gradient. Bench-dried branches were kept cool overnight in a sealed dark bag to enable equilibration of Ψ throughout the branch, which was later verified with a pressure chamber before beginning the fog exposure treatment. Undamaged, individual shoots bearing either peripheral or axial leaves were then removed to yield 5-20 peripheral and 3-5 axial shoots per branch. To capture the full range of peripheral leaf development and age distribution, we used shoots ranging in estimated age from 1 to 7 years. Ends of individual shoots were sealed with Parafilm and weighed before suspending them in a fogging chamber. Following the method of Guzmán-Delgado *et al.* (2017), shoots were placed in a fog-filled chamber and removed at ~20-min intervals. Fogged shoots were immediately blotted dry and weighed, and their final Ψ was recorded. After the fogging, each shoot was carefully dissected and scanned to quantify leaf silhouette area. The series of pre- and post-fog exposure weight-per-area and Ψ measurements were used to generate curves for determination of foliar uptake rate as a function of initial water potential per sample.

Data analysis

Comparison of peripheral and axial leaves – To examine the multivariate differences between peripheral and axial leaves, we used principal components analysis (PCA) of 8 foliar traits (**Table 2.2**). The PCA was performed on peripheral and axial leaves together using a correlation matrix with Euclidean distance. The mean trait skewness was 0.679 and mean kurtosis was 0.683 with all individual-trait values below three. The R package hypervolume() (Blonder, 2018) was used to measure the overlap of peripheral and axial leaves in trait space based on PC axis scores. We tested whether uptake rates, traits, and photosynthetic rates were dependent on leaves being peripheral or axial using Wilcoxon rank sum tests with continuity correction for ties via R (R Core Team).

Quantification of foliar water uptake rates for whole-tree scaling – With data from the fogging experiment, we plotted area-based mass increase per minute (g m^{-2} min^{-1}) against the initial Ψ of each shoot when first exposed to fog, forcing the line through the origin to reflect the lack of uptake in the absence of a Ψ gradient. The resulting linear fits (**Table 2.3**) were used with estimates of peripheral and axial leaf areas to predict uptake in each foliar height-bin using the assumed pre-dawn Ψ (for example, -0.98 MPa at 100 m). Because these values were established per sample at its estimated pre-dawn Ψ, they reflected *in situ* uptake.

Whole-tree scaling and leaf type distribution – Previous research on *Sequoia* involved intensive crown-mapping of trees as well as dissection of representative branches in both unlogged primary forests and previously-logged secondary forests (Sillett *et al.* 2010, 2015, 2018; Kramer *et al.* 2014). Published leaf area estimates reported total leaf area, but during branch dissections of foliage, pliable shoots were measured separately from woody shoots along the height gradient. All leafy twigs up to 1 cm in diameter were separated into three categories: young pliable shoots bearing green leaves (L), older woody shoots bearing green leaves (G), and woody shoots bearing mostly brown leaves (B). We used the L category to estimate peripheral leaf area, and we averaged G and B categories to estimate axial leaf area per branch. These estimates of peripheral and axial leaf areas afforded us opportunities to consider them separately in a scaling exercise and to assess the physiological and ecological implications of their distributions within and among trees growing in different forests. For purposes of whole-tree scaling, we estimated peripheral and axial leaf areas in 5-m height bins for tall individuals in the northern (tree A) and southern (tree B) portion of the species range. Equations for estimating peripheral and axial leaf area fractions were developed for trees in northern and southern primary forests based on previous branch dissections (**Table 2.3**; Sillett *et al.* 2015, Kramer *et al.* 2014). We applied allometric equations to predict total leaf area per height-bin, developed by mapping 114 trees in primary forests

(Sillett *et al.* 2020). We also estimated total peripheral and axial leaf-area for an additional 6 crown-mapped trees up to 116 m tall.

Estimates of leaf area were used to predict uptake of peripheral and axial leaves in each 5-m height bin. To investigate the photosynthetic cost of axial leaf investment we combined existing data on light attenuation with depth in *Sequoia* crowns (Oldham *et al.* 2010, N = 5 trees, 57 inner and outer crown positions) and the photosynthetic response to light availability from peripheral leaves collected at different heights in the same trees (Mullin *et al.* 2009, N = 5 trees, 14 crown positions). For each of the 14 samples with light curves, we predicted photosynthetic output based on local light availability. This approach enabled us to generate a logarithmic curve (**Table 2.3**, **Fig. 2.4**) to serve as a basis for approximating the leaf-area-based photosynthetic potential per height bin. We used these uptake and photosynthesis calculations to create potential-output surfaces for study trees that allowed us to explore variation in leaf-type costs and benefits across the observed range of axial leaf-area investment on individual branches (see **Fig. 2.4**).

Quantification of maximum uptake for trait models – Modeling impacts of leaf traits on foliar water uptake required establishment of sample-specific uptake capacities for comparison. Using mass increase and shoot area data from the fogging experiment, we established a "maximum uptake" value per sample by plotting water absorption (g m^{-2}) against number of minutes each shoot was exposed to fog for sets of peripheral and axial shoots per branch. We did not use any experimental runs with initial weight losses > 10% because we assumed experimenter error (2 runs) and discarded 6 of 248 individual points as outliers based on Cook's distance before fitting logarithmic curves. Only curves yielding rates with errors less than the estimates were retained (final curves: N = 12 peripheral, and 11 axial). For each sample-specific function (Form: $y = m*ln(x)+b$), we used the first derivative at "minute one" (Form: $y' = m*(1/x)$) as "maximum uptake" (g m^{-2}). These values, derived from branch-specific functions, indicate

maximum surface permeability at the start of foliar uptake but do not reflect continuous absorption of water over time, making them unsuitable for estimates of whole-tree uptake.

Structural equation models of uptake rate – A typical goal of structural equation modeling (SEM) is to test the validity of an *a priori* theoretical model by examining how well it approximates relationships (covariance) in a matrix of observations. The assumption that the model is correct (based on knowledge of the system) allows users to estimate the relative causative effects of factors influencing a variable of interest (Grace 2006). In our case, if uptake is a purely physical process, then the underling model explaining variation in foliar uptake rate is Ohm's Law. Rather than testing the validity of this law of physics, we had the potential to fit a fundamentally correct model. Our first goal was to estimate conditionally independent effect sizes of surface resistance and $\Delta\Psi$ on uptake rate by specifying a model for uptake with paths from initial $\Delta\Psi$ and a composite variable representing 'surface resistance' (**Fig. 2.3a**). This modeling approach allowed us to identify a set of traits whose collective effects determine surface resistance. Because the *a priori* model is correct, using prior knowledge of trait-function to identify a combination of leaf surface properties resulting in a good-fitting covariance matrix helped to establish a causal relationship between surface traits and hydraulic resistance.

We selected candidate leaf traits from both the adaxial (peripheral leaves only) and abaxial leaf surfaces to create potential composite variables representing surface resistance in an iterative, leave-one-out approach (surface traits in **Table 2.2**). Beginning with a saturated model containing four traits per leaf side, we removed the worst preforming trait per step, adding a trait back in and trying another if its removal decreased model quality. The final model structure for peripheral leaves was selected because it was the only model where 1) all traits had significant parameters with errors ≤ half the estimates and 2) R^2, χ^2, and comparative fit index (CFI) all suggested an adequate fit (Grace 2006). In most cases, the SEM process relies on a large sample size to obtain model fit. Here we were able to fit a small sample-size model (*i.e.*, N = 10 peripheral leaf uptake values) because of the unusual circumstance

of having a simple, substantially over-identified recursive model with no latent variables, exogenous variables all with very low measurement error, strong correlations with maximum uptake, and perhaps most importantly, a physical law as an *a priori* model. Unfortunately, where modeling was unsuccessful, we could not conclude that it was because the specified process did not describe observed data. Our goal was to understand a process, not to make predictions based on the parameter estimates, so the inability to calculate a reliable RMSEA at small sample sizes was not problematic.

As part of our compositing process for the 'surface resistance' variable, we specified the loading for the first-listed trait causing resistance in each candidate composite. These start values were obtained by first specifying a SEM model where uptake rate was directly predicted by traits selected for defining the new composite variable. We then pre-multiplied the parameter estimate from that initial model by the first-listed trait in the candidate composite variable to specify its start estimate (Grace 2006). To examine the impacts of shared causality between traits and Ψ, we re-fit the single retained model, removing Ψ, and adding height as a predictor of uptake as well as each of the three traits causing resistance. We used maximum likelihood estimators to obtain model fits, and we assessed global and local model fits and complete specification of relationships in models with R^2, χ^2, CFI, and examination of residuals (Grace 2006). This SEM process was repeated for peripheral leaves, axial leaves, and both together, but it was only successful for peripheral leaves. We report path coefficients in units of standard deviation change to indicate their relative effect sizes. The package lavaan() was used for all SEM model specification, fitting, and calculation of fit measures (Rosseel 2012). All statistical analyses were performed in R, and calculations were done in R and Excel.

Results

Comparison of peripheral and axial leaves – Principal components analysis of 8 foliar traits yielded 2 significant axes, retaining 62 % of the variation in peripheral and axial leaf structure. Within

the full leaf trait-space, the separate 8-dimensional hypervolumes occupied by peripheral and axial leaves had zero spatial overlap, further confirming that they belong to two entirely different shoot morphotypes, fully distinguishable on the basis of surface and vascular traits without information on morphology or shoot position. The first principal component (PC1) correlated well with uptake rate (R^2 = 0.45) but only weakly with sample height (R^2 = 0.12). However, when considering points associated only with peripheral leaves, PC1 was strongly related to sample height (R^2 = 0.82) and uptake (R^2 = 0.69). Univariate differences in key vascular traits were suggestive of functional divergence. Peripheral leaves had greater xylem and phloem areas but less transfusion tissue and fewer central fibers than axial leaves (**Fig 2.2c**, **Table 2.2**). Phloem of axial leaves appeared largely non-functional with either occluded cells or, in many cases, cell walls that had grown inward and nearly filled the lumens (**Fig. 2.2d**).

We found that while peripheral leaves were photosynthetic as expected, axial leaves respired slightly more CO_2 than they assimilated in sun or shade (**Table 2.2**), and only 1 of 7 axial shoots exhibited positive net photosynthesis under optimal conditions. Peripheral leaves did not have stomatal conductance rates significantly higher than those of axial leaves, although sample size may have been too small to detect a difference (**Table 2.2**).

Whole-tree uptake scaling and shoot type distribution – Peripheral leaves were capable of foliar water uptake at a rate of 0.12 g m^{-2} min^{-1} ΔMPa^{-1}, while axial leaves could absorb ~ 4X that amount, 0.48 g m^{-2} min^{-1} ΔMPa^{-1} (**Table 2.3**). The largest tree from which we collected shoots for fogging, at 97 m tall with 8909 m^2 of leaf area distributed across a complex crown structure, had the potential to absorb ~ 48 kg hr^{-1} of water at predawn Ψ (Tree A, **Table 2.4**). The smallest tree in our study, Tree E, with 929 m^2 of leaf area distributed across a simple crown structure, had the potential to absorb ~ 4 kg hr^{-1} of water. Axial shoot uptake-contribution varied among trees (**Table 2.4**) and reached up to 31 % of foliar uptake in treetops of dry inland forests. Among the seven additional trees (not used for experimental fogging) for which we estimated peripheral and axial leaf areas, estimated uptake increased with trunk diameter

(*f*-DBH, R^2 = 0.69) due to an increase in both total leaf area and axial fraction (R^2 = 0.45) with this measure of tree size. Among these tall individuals, however, estimated axial fraction decreased with tree height (R^2 = 0.95). The tallest tree (116 m) had only 4 % of its total leaf area in axial leaves. Because of its low proportion of axial leaves, this individual had potential to absorb only ~ 31 kg hr^{-1} during leaf-wetting events despite having 5193 m^2 of projected leaf area. Axial leaf area fraction decreased with height in forests north of 40° latitude but increased with height in forests south of 38° latitude. *Sequoia* trees in the southernmost location (LH) had a greater whole-tree axial leaf area percent (7.4 ± 0.41 %) than did trees growing in northern forests (5.6 ± 0.33 %; **Tables 2.1, 2.3**; **Fig. 2.4**).

Maximum uptake – Both peripheral and axial leaves were capable of foliar uptake at all crown positions, but maximum uptake (initial surface permeability) as derived from sample-specific flux curves, varied among branches. Axial-leaf maximum uptake ($\overline{x}$ = 23.79) at estimated pre-dawn Ψ was significantly greater than the maximum uptake of peripheral leaves ($\overline{x}$ = 7.14, **Table 2.2**). Maximum uptake rate in peripheral leaves increased nonlinearly with start water potential, which was always very close to expected pre-dawn Ψ values estimated from sample height (R^2 = 0.85, **Table 2.3**, **Fig. 2.3c**). In contrast, maximum uptake in axial leaves was unrelated to shoot water potential when fogging began (R^2 < 0.1), though in multi-branch data, uptake (g m^{-2} min^{-1}) was related to Ψ in both shoot types (**Table 2.3**) and used for estimating whole-tree absorption capacity.

Structural equation models (SEM) – We were able to fit a SEM describing maximum uptake in peripheral leaves with a R^2 = 0.955 and a comparative fit index (CFI) of 0.952 (χ^2 of 6.013, df = 4, *P*-value = 0.198; **Fig. 2.3a**). Surface resistance was caused by the collective effects of abaxial stomatal density, abaxial stomatal guard cell length per area, and abaxial surface wax coverage (**Fig. 2.3a**). The effects of the initial Ψ gradient ($\Delta\Psi$) on uptake were ~ 30 % greater than the effects of surface resistance. Because leaf traits can vary in association with height, we examined the importance of shared causality between traits and $\Delta\Psi$ (which was height-based) by removing $\Delta\Psi$ from the model and adding height as a

predictor of all three traits and uptake. The resulting SEM had similar parameter estimates, with an R^2 = 0.938, a very low χ^2 of 0.034 (df = 2, *P*-value = 0.983), and a CFI of 1, but despite the improved fit indicators, comparison of AICc scores indicated that the model with height was half as likely the original SEM with Ψ. We interpret this to mean that even though our final model (shown in **Fig. 2.3a**) misses some of the variation in traits caused by factors associated with height, it is generally correct in elucidating the causes of surface resistance and uptake variation.

We were unable to identify an adequately fit SEM of uptake in axial leaves or axial and peripheral leaves combined. A key leaf trait in both peripheral and axial models, and the trait with the greatest univariate correlation with maximum uptake, was the covering fraction of epicuticular waxes on the abaxial surface (**Fig. 2.3b**). All three traits in the SEM model were from the abaxial leaf surface, and no adaxial traits had strong univariate correlations with maximum uptake.

Discussion

Redwoods meet the contradictory challenges of seasonally dry rainforest environments by allocating photosynthetic and water absorptive functions to leaves on two structurally-specialized shoot types (**Fig. 2.1**, **Table 2.2**), allowing up to 48 kg H_2O hr^{-1} of whole-tree foliar uptake (**Table 2.4**). The photosynthetically-productive peripheral leaves (**Fig. 2.1**) absorb less water than leaves of co-occurring conifers (Kerhoulas *et al.* 2019), but a waxy coating (**Figs. 2.2a**, **2.3b**) and densely packed stomatal plugs may support photosynthesis during extended wet periods at the price of increased surface resistance to water uptake (**Fig. 2.3**). Axial leaves have more than three times the maximum uptake of peripheral leaves (**Table 2.2**), allowing for more rapid foliar water absorption along the valuable woody-axis that supports clusters of peripheral shoots. Axial leaves themselves may be largely non-photosynthetic and have potential maintenance costs (**Table 2.2**, **Fig. 2.2d**). Substantial foliar uptake—in the key woody support structures of all photosynthetic leaves—could permit embolism repair and vascular recharging

(Chin *et al.* 2021), aligning with an ecological strategy of longevity where stress-tolerance in vulnerable distal organs protects the tree as a whole. Uptake of water by thin-barked, leafless twigs may support additional localized recovery (Earles *et al.* 2016). However, surface area of mostly barky twigs < 1 cm diameter, many of which are axial shoots with brown leaves, is 20X less than total leaf surface area (Sillett *et al.* 2015). With a bark uptake rate < 10 % that of peripheral leaves (based on data shown in Earles *et al.* 2016), it seems that bark contributes a small amount to whole-tree uptake capacity.

Foliar water uptake in peripheral leaves behaves according to the expectations of Ohm's Law (**Fig. 2.3a**), suggesting that is a purely physical process dependent on $\Delta\Psi$ as the driving force without the involvement of processes that lower resistance over time (**Fig. 2.3a, c**). Three leaf traits collectively cause surface resistance, and after controlling for $\Delta\Psi$, they explain 96 % of the variation in peripheral-leaf maximum uptake rate. These traits—coverage of visible epicuticular waxes, stomatal density, and guard cell length per area—all respond to environmental signals (Baker 1974, Hadley & Smith 1989, Ashton & Berlyn *et al*. 1992, Gonźales & Ayerbe 2010, Hronkova *et al.* 2015, Salgado-Negret *et al.* 2015), making uptake capacity subject to regional conditions, as in the fern *Polystichum munitum* (Limm & Dawson 2010). Wax coverage in particular varies among samples and is the only trait we found to be a better predictor of uptake variation in peripheral and axial leaves combined (R^2 = 0.64) than within shoot-type. Comparably high uptake rates are not observed for peripheral leaves with wax covering fractions as low as that of axial leaves (**Fig. 2.3b**) showing the influence of other traits. Interestingly, maximum axial leaf uptake is uncorrelated with $\Delta\Psi$ (R^2 < 0.00001), unlike uptake rates over time (**Table 2.3**). This implies that other passive or active mechanisms may impact surface permeability to water at the beginning of uptake. Uptake variation may be related to many factors not explored here, including a drop in surface resistance with increasing hydration of cuticular waxes, multiple physiological or physical factors that vary with leaf hydration, increases in internal capacity to transport water related to change in cell volume, or increases in aquaporin activity (Ohrui *et al.* 2007, Laur & Hacke 2014). In addition, the

abundance of epiphyllic organisms on the sheltered surface of decurrent axial leaves may further enhance uptake capacity (**Fig. 2.2b**; Holder 2011).

Axial leaves do not appear to contribute photosynthetically, thus costs of their construction and maintenance come at the expense of additional peripheral leaf area (**Table 2.2**, **Fig. 2.4**). Conversely, if the green axial shoots were converted to bark, that same surface area would absorb ~ $1/50^{th}$ of the water axial leaves are capable of contributing (Earles *et al.* 2016), a considerable hydraulic cost. It appears that something about axial leaves being green, whether lack of surface suberization, the presence of living parenchyma, or other factors, promotes uptake. Outsized investment in transfusion tissue area in axial leaves (**Table 2.2**) likely serves a protective function (Chin Chapter 1), only while the leaf lives. While the fractional investment in axial leaves decreases with height in northern forests, the southernmost forest shows an opposite trend—concentrating axial leaves in the sunny treetops (**Fig. 2.4**). Because treetop peripheral leaves have the greatest potential for photosynthetic contribution, the construction of axial leaves has a higher tradeoff-cost per area in southern forests (**Fig. 2.4**). Treetop axial leaves may be a necessity in relatively dry forests where summertime leaf wetting events are less frequent, of shorter duration, and trees are likely to be operating closer to their hydraulic limits (PRISM 2020, **Table 2.1, Fig. 2.4**). Distance from the dew-point could be of particular importance in driving the differences in axial-leaf investment among locations (**Tables 2.1, 2.3, 2.4, Fig. 2.4**), because leaf-wetting due to condensation may better reach the entire depth of the crown than can small quantities of precipitation.

The trade-off between axial and peripheral leaf construction is not solely a reflection of the availability of light and aerial water. It is complicated by the fact that axial shoots provide support for clusters of peripheral shoots, and axial leaves are maintained as green for varying lengths of time. In treetops, light availability should promote the fractional investment in peripheral shoot area (lower ratio of axial to peripheral green leaf area). However, where precipitation is at a premium and dew points

may be reached infrequently (i.e. southern forests, **Table 2.1**, **Fig. 2.4**), trees maintain a higher axial leaf area fraction. When predicted axial leaf area investment is considered for individual trees, both crown structure and geographic location have large potential impacts on axial contribution to foliar uptake rate (**Fig. 2.4**). In our study trees, axial leaves contributed an extra 18-29 % to whole-tree foliar uptake. Predicted patterns of axial leaf investment lead to a larger uptake benefit per photosynthetic cost in northern rainforests, and greater uptake per leaf area in dry southern forests (**Table 2.4**).

Balancing axial and peripheral leaf areas allows redwoods to protect key structures during dry summers and still avoid photosynthetic losses during prolonged wet periods by freeing peripheral leaves to avoid excessive water accumulation and maintain high stomatal conductance (Smith & McClean 1989, Hanba *et al.* 2004, Ambrose *et al.* 2010, Gerlein-Safidi *et al.* 2018). Dimorphic division of labor promotes the longevity of shoot clusters, thus reducing their cost-benefit ratio, and allows for year-round carbon acquisition. A longevity-focused life history requires the ability to recover from infrequent droughts. In the relatively dry forests of the southern range, the need for hydraulic recovery may force prioritization of foliar water uptake through costly investment in treetop axial-leaf construction (**Fig. 2.4**). Surface hydraulic resistance is an underlying physical property caused by visible traits (**Fig. 2.3a, b**), and it is these micro-scale features of leaves that respond to environmental signals and vary within and among trees (Rosado *et al*. 2010, Binks *et al.* 2019, Chin & Sillett 2019)—likely driving further regional variation in uptake capacity. Regional uptake differences may have large-scale impacts on forest hydrology and climate sensitivity (Holder 2007b, Konrad *et al.* 2012, Shreel & Steppe 2020). Broadleaved trees in seasonally wet forests are able to separate foliar uptake and gas exchange by having an absorptive adaxial surface, and a hydrophobic abaxial surface bearing stomata (Smith & McClean 1989, Holder 2007a, Eller *et al.* 2013, Fernandez *et al.* 2014). In conifers, limits to leaf width and shape imposed by a single vein (Zwieniecki *et al.* 2004) may make it harder for the abaxial surface of their needle-like leaves to remain dry if water accumulates on the adaxial surface to allow foliar uptake (Rosado *et al*. 2010,

Limm & Dawson 2010, Fernández *et al.* 2014). Shoot dimorphism solves this problem and potentially allows *Sequoia* the flexibility to optimize investments in uptake capacity and photosynthesis across vertical and latitudinal gradients, supporting both growth and longevity.

Figure 2.1. The peripheral and axial leaves of redwoods. Redwood branches are heteroblastic with an abrupt metamorphic change between dimorphic shoot types (transition visible in left panel). In panel on right, peripheral shoots (left column), which make up the vast majority of leaf area, vary dramatically with height but always have less decurrent leaves and are pliable for the first few years of development. Axial shoots (right column) are thick, woody central shoot-cluster leaders supporting many peripheral shoots. They have highly decurrent leaves at all heights and never arise from peripheral shoots.

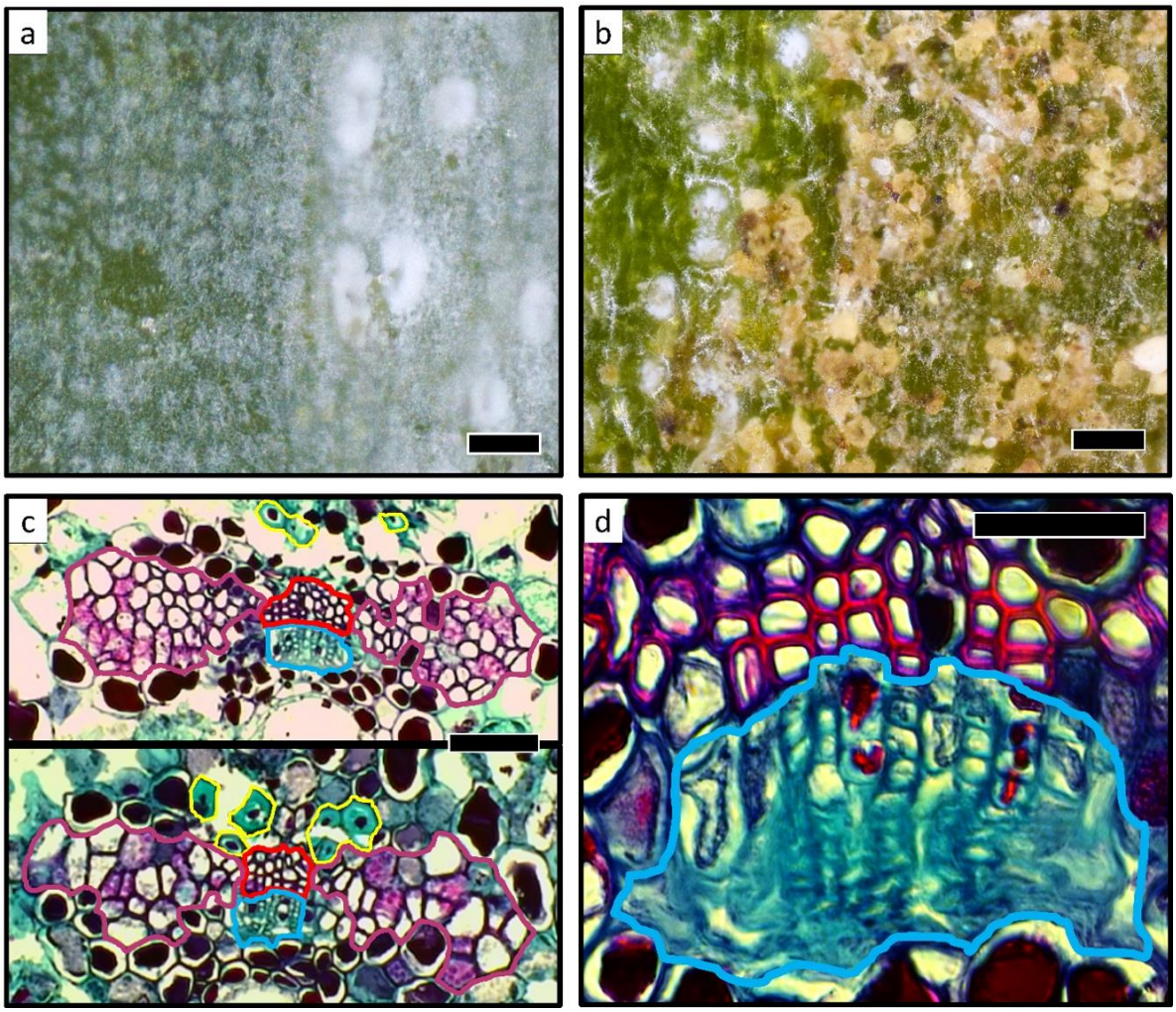

Figure 2.2. Traits of peripheral and axial leaves. a) In waxy abaxial surface of peripheral leaves, white spots are stomatal plugs. Scale bar = 0.05 mm. **b)** Sheltered adaxial surfaces of axial leaves host abundant epiphyllic organisms. Scale bar = 0.05 mm. **c)** Vascular anatomy of peripheral leaves (top) and axial leaves (bottom). Outlines: purple = transfusion tissue, yellow = central fibers, red = xylem, blue = phloem. Scale bar = 0.1 mm. **d)** Phloem of axial leaves (blue outline) has many occluded cells and fused walls, suggesting reduced sugar-transport functionality. Scale bar = 0.035 mm.

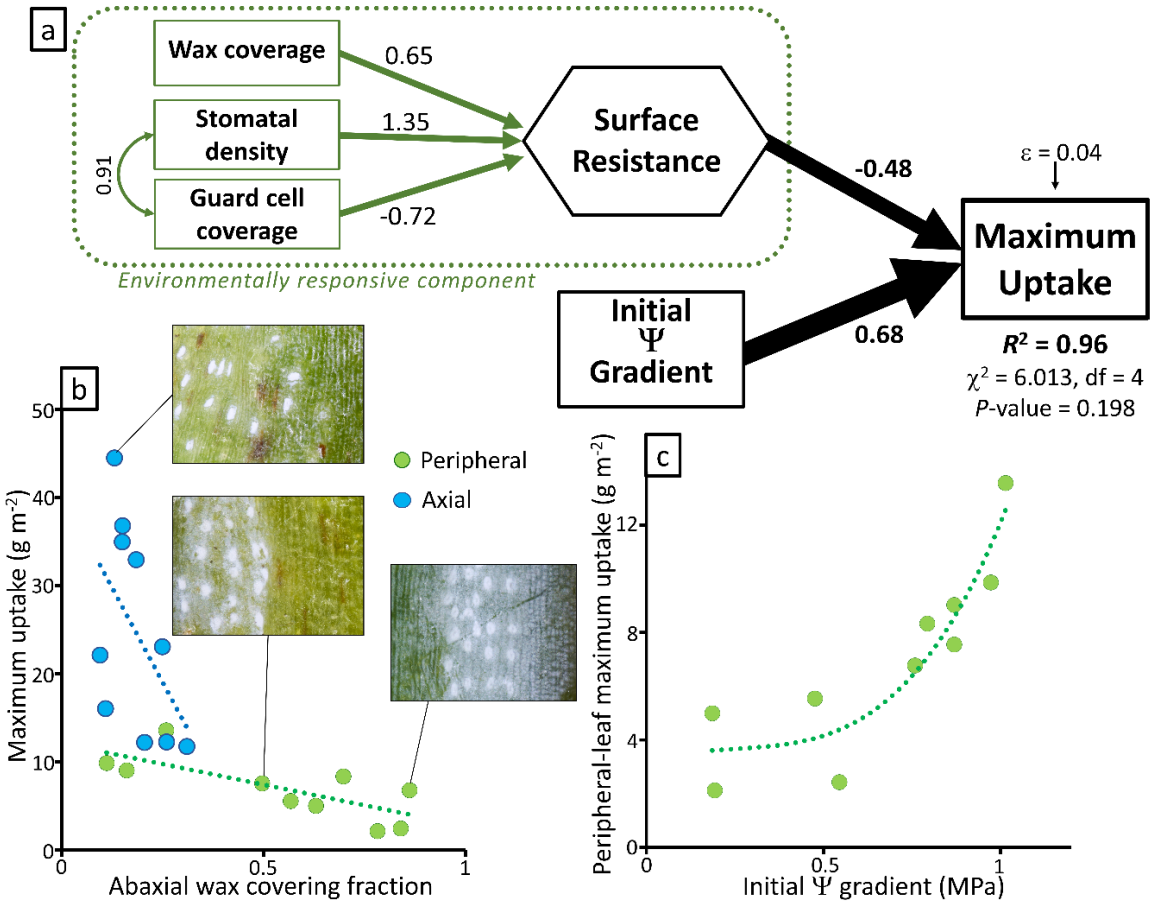

Figure 2.3. What causes variation in foliar uptake potential? a) Based on Ohm's Law, this structural equation model characterizes the determination of peripheral-leaf maximum uptake by leaf surface resistance and Ψ gradient (mimicking the predawn Ψ gradient due to gravity). Black arrow thickness shows relative effect sizes. Surface resistance is caused by composite effects of three leaf traits (green arrows). Dotted green box designates portion of model that may respond to environmental signals through acclimation or long term regional adaption of leaf traits. Arrows indicate directions of causality. Small curved green arrow (far left) represents covariance of stomatal density and guard cell coverage. Path coefficients are relative effect sizes in units of standard deviation. **b)** Relationship between abaxial wax covering fraction and uptake rate in peripheral leaves (R^2 = 0.56) and axial leaves (R^2 = 0.26). **c)** In peripheral, but not axial, leaves maximum uptake increases with the magnitude of the initial Ψ gradient (R^2 = 0.85).

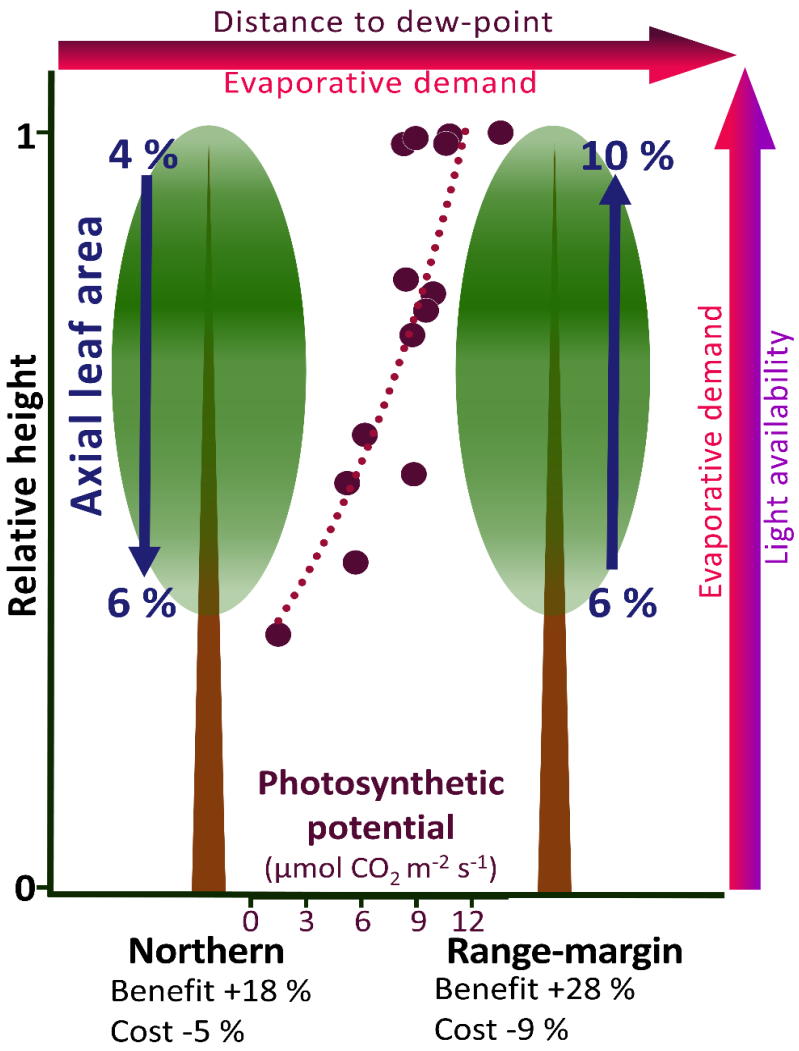

Figure 2.4. **Geographic variation in foliar water uptake requirements and axial shoot distribution**. Conceptual model illustrating how multiscale environmental variation within and among *Sequoia* forests could necessitate prioritization of axial leaf area in upper crowns of trees growing in southern range. In treetops, axial leaves have their greatest cost in lost peripheral-leaf photosynthetic opportunity but also make their greatest uptake contribution relative to peripheral leaves. Latitudinal decreases in the distance between minimum summertime temperatures and the dew-point, and increases in precipitation, indicate that southern forests have less frequent summertime leaf wetting events (**Table 2.1**). Greater evaporative demand at the southern and eastern range margins suggests that these infrequent condensation events are sustained for shorter periods, while vertical gradients in evaporative demand imply that treetops experience the shortest leaf-wetting events of all. The need to take full advantage of rare and transient leaf wetness, to allow hydraulic repair despite the gravitational Ψ gradient, could explain the relatively high treetop axial-fraction on the southern range-margin and supports the notion that the ability to improve water status may have an overall positive effect on CO_2 acquisition. Using Tree C (**Table 2.4**) as a model, we show estimated axial leaf areas for northern trees (> 40° latitude) and trees on range-margins based on LH location (36° latitude, **Table 2.1**). Color shading of tree crowns indicates the relativized distribution of Tree C's total leaf area in 5-m height-bins. Approximate axial-shoot foliar uptake benefit and CO_2 lost-acquisition cost shown below.

Table 2.1. Sets of parameters used in this study, data sources and study locations ranked by latitude. Climate data are 30-year monthly normals 1981-2010 with 800 m spatial resolution, dew-point is the maximum temperature for condensation, VPD is vapor pressure deficit (climate data from PRISM 2020).

Parameter	Data sources	Previously publication	N	Locations
A Leaf traits in Table 2	All 11 traits are from the current study	None	6 trees, see Table 2	Range wide
B Predicted photosynthesis	*Both sources used the same 5 trees, we use the combined data to estimate the output of lateral leaves at different heights*			
Light response curves	Mullin et al. 2009	Summary data for 3 height-bins	14 heights, 3 curves each	North
Light availability	Oldham et al. 2010	Points shown, equation not provided	57 crown positions	North
C Leaf area fractions	Sillett et al. 2010,2015; Kramer et al. 2014	Total leaf area, not lateral/axial fractions	93 branches	7 Range wide

Location	Parameters Sampled	Latitude	Annual Rainfall (mm)	Mean Monthly Summer Rainfall (mm)	Mean Summer Dewpoint (°C)	Min Summer Temperature (°C)	Max Summer VPD (hPa)	Max Summer Temperature (°C)
JS*	A, C	41.8	2003	24.98	11.23	10.33	14.32	22.43
PC*	C	41.4	1648	18.88	10.43	9.33	10.92	20.53
RNP*	C	41.2	1757	19.84	10.63	10.17	13.51	23.00
HR*	B, C	40.3	1722	10.74	9.70	10.40	28.20	28.77
RRR◊	A	38.6	1356	4.11	10.70	11.10	20.54	25.33
ATP¤	A	38.4	1100	3.47	9.37	12.37	28.90	28.80
SPT◊	C	38	1061	3.42	10.53	11.43	21.31	26.10
RRP¤	A	37.8	727	3.04	10.43	12.10	19.29	24.97
BB◊	C	37.2	898	4.18	10.63	10.50	21.25	26.60
SCM◊	A	37.1	1487	4.49	7.53	13.70	24.11	26.63
LH¤	C	36.1	868	1.84	8.97	12.27	20.10	24.43

* = Northern Sites, ◊ = Central Sites, ¤ = Range-margins

Table 2.2. Definitions of foliar traits used in this study and their values and differences between peripheral and axial shoots of *Sequoia sempervirens*. Surface traits are for abaxial side of leaf, large errors around means reflect broad morphological diversity of *Sequoia* leaves (see **Fig 1**). All 8 surface and vascular traits are also used in PCA.

			Peripheral Leaves		Axial Leaves			
Trait	**Definition**	**Units**	**N**	**Mean ± SE**	**N**	**Mean ± SE**	**W**	***P*-value**
Physiological								
Maximum Uptake	Peak surface permeability to water	$g\ m^2$	11	7.14 (± 13.6 %)	10	23.79 (± 14.8 %)	129	< 0.0001
Photosynthesis	CO_2 assimilated	$\mu mol\ m^2\ sec^{-1}$	5	4.222 (± 20.3 %)	7	-0.1994 (± 68.7 %)	35	0.0025
Stomatal conductance	H_2O lost	$mol\ m^2\ sec^{-1}$	5	0.0339 (± 19.5 %)	7	0.0155 (± 28.4 %)	30	0.0480
Surface								
Visible wax coverage	Wax area per leaf area	fraction	13	0.5625 (± 13.2 %)	10	0.2338 (± 15.1 %)	143	0.0019
Guard cell length	Mean guard cell length	mm	10	0.0352 (± 4.5 %)	10	0.027 (± 9.6 %)	104	0.0169
Stomatal density	Stomata per leaf area	$count\ mm^{-2}$	13	48.88 (± 12.2 %)	10	36.03 (± 18.1 %)	91	0.1151
Guard cell covering fraction	Guard cell length per leaf area	$mm\ mm^{-2}$	10	1.6734 (± 11.5 %)	10	0.9639 (± 20.6 %)	102	0.0210
Vascular								
Transfusion tissue area	Cross-sectional area	mm^2	11	0.0127 (± 9.4 %)	10	0.0207 (± 13.5 %)	22	0.0065
Xylem area	Cross-sectional area	mm^2	11	0.0028 (± 7.2 %)	10	0.0018 (± 11.1 %)	107	0.0100
Phloem area	Cross-sectional area	mm^2	11	0.0032 (± 9.4 %)	10	0.0021 (± 19.0 %)	102	0.0234
Central fibers	Number per cross section	count	11	0.62 (± 53.2 %)	10	3.1 (± 16.1 %)	16	0.0016

Table 2.3. Equations developed for approximations of *Sequoia sempervirens* whole-tree foliar uptake and photosynthetic potential. Where RMSE is root mean square error and CV is the coefficient of variation (RMSE/mean) expressed as a percent. Models are not intended for reliable prediction.

Predicted variable	Predictor (V)	a	b	N	R^2	RMSE	CV	*P*-value	Form
% Axial leaf area, Northern primary forests	Relative height	-4.7753	9.0622	54	0.25	1.667	30	0.0001	aV + b
% Axial leaf area, Marginal forests (from LH)	Relative height	7.907	2.097	12	0.44	0.978	13	0.0193	aV + b
Photosythetic rate (μmol CO_2 m^{-2} s^{-1})	Relative height	7.3679	10.853	14	0.74	1.440	19	< 0.0001	a ln(V) + b
Axial-leaf foliar water uptake (g m^{-2} min^{-1})	Initial Y (MPa)	0.45585	–	58	0.60	0.237	91	< 0.0001	aV + 0
Peripheral-leaf foliar water uptake (g m^{-2} min^{-1})	Initial Y (MPa)	0.09708	–	174	0.26	0.104	185	< 0.0001	aV + 0

Table 2.4. Individual *Sequoia sempervirens* trees used for measurements of physiological and anatomical traits of peripheral and axial shoots (Parameter A, **Table 2.1**). Trees varied widely in size and age, *f*-DBH is functional diameter at breast height (1.37 m), crown depth is extent of live foliage from treetop to base of live crown, size metrics estimated from existing allometric equations. Whole-tree foliar uptake and photosynthetic potential (peripheral leaves only) were approximated using equations in **Table 2.3**. Location details in **Table 2.1**, trees ranked by latitude.

Tree	Location	Height (m)	f-DBH (cm)	Crown Depth (m)	Crown Radius (m)	Crown Volume (m^3)	Tree Age (yr)	Biomass (Mg)	Total Leaf Area (m^2)	Leaves (millions)	Axial Leaf Area (%)	Estimated Foliar Uptake (kg H_2O hr^{-1})	Estimated Photosynthetic Potential (kg CO_2 hr^{-1})	Axial Uptake Contribution (%)
A	JS	97.9	750	77.4	12.4	25085	1267 (± 8.5 %)	469 (± 2.2 %)	8909 (± 9.9 %)	1006 (± 8.9 %)	5.8	48	10	20
B	RRR	93.9	276	58.4	9.6	11155	543 (± 7.2 %)	53 (± 2.6 %)	2606 (± 12.0 %)	260 (± 11.5 %)	8	16	3	27
C	RRR	98.2	212	43.2	9.1	7402	650 (± 2 %)	40 (± 2.3 %)	1929 (± 10.2 %)	191 (± 9.8 %)	8	13	3	27
D	ATP	70.2	184	32.4	8.4	3586	238 (± 7.2 %)	16 (± 0.4 %)	2056 (± 3.6 %)	193 (± 4.0 %)	7.9	9	3	27
E	RRP	64.0	129	24.6	6.0	1380	148 (± 2 %)	10 (± 0.5 %)	929 (± 5.0 %)	95 (± 4.9 %)	8.3	4	1	28
F	SCM	107.3	352	80.5	9.4	15016	874 (± 0.2 %)	108 (± 2.1 %)	3642 (± 10.3 %)	371 (± 9.7 %)	8	24	4	27

Literature Cited in Chapter 2

Ambrose, A.R., Sillett, S.C., Koch, G.W., Van Pelt, R., Antoine, M.E. and Dawson, T.E., 2010. Effects of height on treetop transpiration and stomatal conductance in coast redwood (Sequoia sempervirens). *Tree Physiology*, 30:1260-1272.

Aparecido, L.M., Miller, G.R., Cahill, A.T. and Moore, G.W., 2017. Leaf surface traits and water storage retention affect photosynthetic responses to leaf surface wetness among wet tropical forest and semiarid savanna plants. *Tree physiology*, 37:1285-1300.

Ashton, P.M.S. and Berlyn, G.P., 1992. Leaf adaptations of some Shorea species to sun and shade. *New Phytologist*, 121:587-596.

Baker, E.A., 1974. The influence of environment on leaf wax development in Brassica oleracea var. gemmifera. *New Phytologist*, 73:955-966.

Barthlott, W. and Neinhuis, C., 1997. Purity of the sacred lotus, or escape from contamination in biological surfaces. *Planta*, 202:1-8.

Berry, Z.C. and Goldsmith, G.R., 2020. Diffuse light and wetting differentially affect tropical tree leaf photosynthesis. *New Phytologist*, 225:143-153.

Berry, Z.C., Emery, N.C., Gotsch, S.G. and Goldsmith, G.R., 2019. Foliar water uptake: processes, pathways, and integration into plant water budgets. *Plant, cell & environment*, 42:410-423.

Binks, O., Mencuccini, M., Rowland, L., da Costa, A.C., de Carvalho, C.J.R., Bittencourt, P., Eller, C., Teodoro, G.S., Carvalho, E.J.M., Soza, A. and Ferreira, L., 2019. Foliar water uptake in Amazonian trees: Evidence and consequences. *Global change biology*, 25:2678-2690.

Blonder, B. (2018). *hypervolume: High dimensional geometry and set operations using kernel density estimation, support vector machines, and convex hulls*. Retrieved from https://cran.r-project.org/package=hypervolume

Breshears, D.D., McDowell, N.G., Goddard, K.L., Dayem, K.E., Martens, S.N., Meyer, C.W. and Brown, K.M., 2008. Foliar absorption of intercepted rainfall improves woody plant water status most during drought. *Ecology*, 89:41-47.

Burgess, S.S.O. and Dawson, T.E., 2004. The contribution of fog to the water relations of Sequoia sempervirens (D. Don): foliar uptake and prevention of dehydration. *Plant, Cell & Environment*, 27:1023-1034.

Chin, A.R. and Sillett, S.C., 2016. Phenotypic plasticity of leaves enhances water-stress tolerance and promotes hydraulic conductivity in a tall conifer. *American journal of botany*, 103:796-807.

Chin, A.R. and Sillett, S.C., 2019. Within-crown plasticity in leaf traits among the tallest conifers. *American Journal of Botany*, 106:174-186.

Clark, J.W. and Scheffer, T.C., 1983. Natural decay resistance of the heartwood of coast redwood Sequoia sempervirens (D. Don) Endl. *Forest Products Journal*, 33:15-20.

Davies, N.T., Wu, H.F. and Altaner, C.M., 2014. The chemistry and bioactivity of various heartwood extracts from redwood (Sequoia sempervirens) against two species of fungi. *New Zealand Journal of Forestry Science*, 44:17.

Dawson, T.E. and Goldsmith, G.R., 2018. The value of wet leaves. *New Phytologist*, 219:1156-1169.

Eller, C.B., Lima, A.L. and Oliveira, R.S., 2013. Foliar uptake of fog water and transport belowground alleviates drought effects in the cloud forest tree species, D rimys brasiliensis (W interaceae). *New Phytologist*, 199:151-162.

Eller, C.B., Lima, A.L. and Oliveira, R.S., 2016. Cloud forest trees with higher foliar water uptake capacity and anisohydric behavior are more vulnerable to drought and climate change. *New Phytologist*, 211:489-501.

Emery, N.C., 2016. Foliar uptake of fog in coastal California shrub species. *Oecologia*, 182:731-742.

Espinosa-García, F.J. and Langenheim, J.H., 1991. Effects of sabinene and γ-terpinene from coastal redwood leaves acting singly or in mixtures on the growth of some of their fungus endophytes. *Biochemical systematics and ecology*, 19:643-650.

Feild, T.S., Zwieniecki, M.A., Donoghue, M.J. and Holbrook, N.M., 1998. Stomatal plugs of Drimys winteri (Winteraceae) protect leaves from mist but not drought. *Proceedings of the National Academy of Sciences*, 95:14256-14259.

Fernández, V., Sancho-Knapik, D., Guzmán, P., Peguero-Pina, J.J., Gil, L., Karabourniotis, G., Khayet, M., Fasseas, C., Heredia-Guerrero, J.A., Heredia, A. and Gil-Pelegrín, E., 2014. Wettability, polarity, and water absorption of holm oak leaves: effect of leaf side and age. *Plant Physiology*, 166:168-180.

Fritz, E., 1931. The role of fire in the redwood region. *Journal of Forestry*, 29:939-950.

Gerlein-Safdi, C., Koohafkan, M.C., Chung, M., Rockwell, F.E., Thompson, S. and Caylor, K.K., 2018. Dew deposition suppresses transpiration and carbon uptake in leaves. *Agricultural and Forest Meteorology*, 259:305-316.

González, A. and Ayerbe, L., 2010. Effect of terminal water stress on leaf epicuticular wax load, residual transpiration and grain yield in barley. *Euphytica*, 172:341-349.

Gotsch, S.G., Nadkarni, N., Darby, A., Glunk, A., Dix, M., Davidson, K. and Dawson, T.E., 2015. Life in the treetops: ecophysiological strategies of canopy epiphytes in a tropical montane cloud forest. *Ecological Monographs*, 85:393-412.

Grace, J.B., 2006. *Structural equation modeling and natural systems*. Cambridge University Press.

Guzmán-Delgado, P., Mason Earles, J. and Zwieniecki, M.A., 2018. Insight into the physiological role of water absorption via the leaf surface from a rehydration kinetics perspective. *Plant, cell & environment*, 41:1886-1894.

Hadley, J.L. and Smith, W.K., 1989. Wind erosion of leaf surface wax in alpine timberline conifers. *Arctic and Alpine Research*, 21:392-398.

Hanba, Y.T., Moriya, A. and Kimura, K., 2004. Effect of leaf surface wetness and wettability on photosynthesis in bean and pea. *Plant, Cell & Environment*, 27:413-421.

Holder, C.D., 2007a. Leaf water repellency as an adaptation to tropical montane cloud forest environments. *Biotropica*, 39:767-770.

Holder, C.D., 2007b. Leaf water repellency of species in Guatemala and Colorado (USA) and its significance to forest hydrology studies. *Journal of Hydrology*, *336*(1-2), pp.147-154

Holder, C.D., 2011. The relationship between leaf water repellency and leaf traits in three distinct biogeographical regions. *Plant Ecology*, 212:1913.

Hronková, M., Wiesnerová, D., Šimková, M., Skůpa, P., Dewitte, W., Vráblová, M., Zažímalová, E. and Šantrůček, J., 2015. Light-induced STOMAGEN-mediated stomatal development in Arabidopsis leaves. *Journal of experimental botany*, 66:4621-4630.

Ishibashi, M. and Terashima, I., 1995. Effects of continuous leaf wetness on photosynthesis: adverse aspects of rainfall. *Plant, Cell & Environment*, 18:431-438.

Jones, C.S., 1999. An essay on juvenility, phase change, and heteroblasty in seed plants. *International Journal of Plant Sciences*, 160:S105-S111.

Jura-Morawiec, J. and Marcinkiewicz, J., 2020. Wettability, water absorption and water storage in rosette leaves of the dragon tree (Dracaena draco L.). *Planta*, 252:1-8.

Kerhoulas, L.P., Weisgrau, A.S., Hoeft, E.C. and Kerhoulas, N.J., 2020. Vertical gradients in foliar physiology of tall Picea sitchensis trees. *Tree Physiology*, 40:321-332.

Konrad, W., Ebner, M., Traiser, C. and Roth-Nebelsick, A., 2012. Leaf surface wettability and implications for drop shedding and evaporation from forest canopies. *Pure and Applied Geophysics*, 169:835-845.

Kramer, R.D., Sillett, S.C. and Carroll, A.L., 2014. Structural development of redwood branches and its effects on wood growth. *Tree physiology*, 34:314-330.

Laur, J. and Hacke, U.G., 2014. Exploring Picea glauca aquaporins in the context of needle water uptake and xylem refilling. *New Phytologist*, 203:388-400.

Limm, E.B. and Dawson, T.E., 2010. Polystichum munitum (Dryopteridaceae) varies geographically in its capacity to absorb fog water by foliar uptake within the redwood forest ecosystem. *American Journal of Botany*, 97:1121-1128.

Mason Earles, J., Sperling, O., Silva, L.C., McElrone, A.J., Brodersen, C.R., North, M.P. and Zwieniecki, M.A., 2016. Bark water uptake promotes localized hydraulic recovery in coastal redwood crown. *Plant, cell & environment*, 39:320-328.

Neinhuis, C. and Barthlott, W., 1997. Characterization and distribution of water-repellent, self-cleaning plant surfaces. *Annals of botany*, 79:667-677.

Ohrui, T., Nobira, H., Sakata, Y., Taji, T., Yamamoto, C., Nishida, K., Yamakawa, T., Sasuga, Y., Yaguchi, Y., Takenaga, H. and Tanaka, S., 2007. Foliar trichome-and aquaporin-aided water uptake in a drought-resistant epiphyte Tillandsia ionantha Planchon. *Planta*, 227:47-56.

Oldham, A.R., Sillett, S.C., Tomescu, A.M. and Koch, G.W., 2010. The hydrostatic gradient, not light availability, drives height-related variation in Sequoia sempervirens (Cupressaceae) leaf anatomy. *American Journal of Botany*, 97:1087-1097.

PRISM 2020. PRISM Climate Group, Northwest Alliance for Computation Science and Engineering. "Norm81m" dataset.

Rosado, B.H.P., Oliveira, R.S. and Aidar, M.P.M., 2010. Is leaf water repellency related to vapor pressure deficit and crown exposure in tropical forests?. *Acta Oecologica*, 36:645-649.

Rosseel Y (2012). "lavaan: An R Package for Structural Equation Modeling." Journal of Statistical Software, 48:1-36.

Rundel, P.W., 1982. Water uptake by organs other than roots. In *Physiological plant ecology II* (pp. 111-134). Springer, Berlin, Heidelberg.

Salgado-Negret, B., Canessa, R., Valladares, F., Armesto, J.J. and Pérez, F., 2015. Functional traits variation explains the distribution of Aextoxicon punctatum (Aextoxicaceae) in pronounced moisture gradients within fog-dependent forest fragments. *Frontiers in plant science*, 6:511.

Schreel, J.D. and Steppe, K., 2020. Foliar water uptake in trees: negligible or necessary?. *Trends in Plant Science*.

Schreel, J.D., von der Crone, J.S., Kangur, O. and Steppe, K., 2019. Influence of drought on foliar water uptake capacity of temperate tree species. *Forests*, 10:562.

Sillett, S.C., Kramer, R.D., Van Pelt, R., Carroll, A.L., Campbell-Spickler, J. and Antoine, M.E., 2021. Comparative development of the four tallest conifer species. *Forest Ecology and Management*, 480:118688.

Sillett, S.C., Van Pelt, R., Carroll, A.L., Campbell-Spickler, J. and Antoine, M.E., 2020. Aboveground biomass dynamics and growth efficiency of Sequoia sempervirens forests. *Forest Ecology and Management*, 458:117740.

Sillett, S.C., Antoine, M.E., Campbell-Spickler, J., Carroll, A.L., Coonen, E.J., Kramer, R.D., Scarla, K.H., 2018. Manipulating tree crown structure to promote old-growth characteristics in second-growth redwood forest canopies. *Forest Ecology and Management*, 417:77-89.

Sillett, S.C., Van Pelt, R., Carroll, A.L., Kramer, R.D., Ambrose, A.R. and Trask, D.A., 2015. How do tree structure and old age affect growth potential of California redwoods?. *Ecological Monographs*, 85:181-212.

Sillett, S.C., Van Pelt, R., Koch, G.W., Ambrose, A.R., Carroll, A.L., Antoine, M.E. and Mifsud, B.M., 2010. Increasing wood production through old age in tall trees. *Forest Ecology and Management*, 259:976-994.

Simonin, K.A., Santiago, L.S. and Dawson, T.E., 2009. Fog interception by Sequoia sempervirens (D. Don) crowns decouples physiology from soil water deficit. *Plant, Cell & Environment*, 32:882-892.
Limm, E.B., Simonin, K.A., Bothman, A.G. and Dawson, T.E., 2009. Foliar water uptake: a common water acquisition strategy for plants of the redwood forest. *Oecologia*, 161:449-459.
Smith, W.K. and McClean, T.M., 1989. Adaptive relationship between leaf water repellency, stomatal distribution, and gas exchange. *American Journal of Botany*, 76:465-469.
Steppe, K., Vandegehuchte, M.W., Van de Wal, B.A., Hoste, P., Guyot, A., Lovelock, C.E. and Lockington, D.A., 2018. Direct uptake of canopy rainwater causes turgor-driven growth spurts in the mangrove Avicennia marina. *Tree physiology*, 38:979-991.
Van Pelt, R., Sillett, S.C., Kruse, W.A., Freund, J.A. and Kramer, R.D., 2016. Emergent crowns and light-use complementarity lead to global maximum biomass and leaf area in Sequoia sempervirens forests. *Forest Ecology and Management*, 375:279-308.
Yates, D.J. and Hutley, L.B., 1995. Foliar uptake of water by wet leaves of Sloanea woollsii, an Australian subtropical rainforest tree. *Australian Journal of Botany*, 43:157-167.
Zimmermann, M.H., 1983. *Xylem structure and the ascent of sap*. Springer Science & Business Media.
Zwieniecki, M.A., Boyce, C.K. and Holbrook, N.M., 2004. Functional design space of single-veined leaves: role of tissue hydraulic properties in constraining leaf size and shape. *Annals of Botany*, 94:507-513.

Chapter 3

Environmentally responsive epidermal traits control foliar water uptake capacity

Foliar water uptake is a capability of many, if not most, terrestrial plants, occurring across taxa and biomes (Rundel 1982, Dawson & Goldsmith 2018, Berry *et al.* 2019). Capacity for foliar uptake varies not only among and within species, but even among the leaves of individual plants suggesting that uptake potential may be swayed by subtle variation in leaf structure (Limm & Dawson 2010, Chin Chapter 2). Among the best-studied species capable of absorbing water when leaves are wet, is coast redwood, *Sequoia sempervirens* (Burgess & Dawson 2004, Simonin *et al.* 2009, Chin Chapter 1, 2). Ability to obtain water without relying on soil sources allows *Sequoia* and other plants to maintain photosynthetic activity, increase growth rates, and recover from water stress during dry summers when leaves may become wet due to fog, condensation, or occult precipitation (Simonin *et al.* 2009, Dawson & Goldsmith 2018, Chin Chapter 1). Dimorphic shoots, one with a very high uptake rate, allow *Sequoia* to acclimate absorptive capacity of their crowns to regional climatic conditions (Chin Chapter 2). However, biophysical and morphological features of leaf surfaces create hydraulic resistance that sets limits on foliar uptake in *Sequoia* by influencing how leaves interact with water (Chin Chapter 2).

Traits causing surface resistance have unknown potential to respond to climatic variation. Such trait variation could have profound impacts on tree performance and forests hydraulics by influencing interception, holding, and evaporation of water from canopy surfaces (Azevedo & Morgan 1974, Holder 2007, Konrad *et al.* 2012). *Sequoia* leaves have the broadest range of multivariate within-crown phenotypic plasticity of any conifer measured (Chin & Sillett 2019), but this does not guarantee environmentally sensitive uptake capacity within a given height-class or among sites. Beyond the potential for wide-ranging phenotypic variation within trees, each individual trait has an innate level of developmental plasticity, a “response repertoire” bounded by the physical, functional, and genotypic

limits constraining its acclimation (Sultan 2017). Can climatic conditions alter leaf surface structure and properties in such a way as to influence uptake capacity? Regardless of development, the exact pathway by which water crosses the leaf surface is unverified in *Sequoia,* thus water might be absorbed through the cuticle, stomata, or both (Burgess & Dawson, 2004, Eller *et al.* 2013, Berry *et al.* 2019, Boanares *et al.* 2018, Guzmán-Delgado *et al.* 2021). Lack of knowledge in this basic area makes it difficult to target traits for ecological monitoring or predict climatically induced acclimations in leaf structure that may alter tree-water interactions on regional scales.

Only a limited number of leaf surface-traits have been explored in *Sequoia*, with leaf epidermal anatomy and wettability entirely uninvestigated (Chin Chapter 2). Understanding the importance and developmental stability of leaf traits requires the exploration of uptake parameters across a range of leaf form, while focusing on a single model species can minimize confounding factors that may hinder interpretation of trait-uptake relationships. We hypothesize that if barriers to water entry at the surface of the leaf dominate the series of resistances in the uptake pathway, then superficial traits such as epicuticular wax and stomatal size, not internal anatomical features, will drive variation in the kinetic parameters of foliar water uptake. Further, traits hindering or facilitating uptake should be species-specific and reflective of the uptake pathway, for example, if water enters *Sequoia* leaves through stomata, then we would expect a positive relationship between stomatal coverage and uptake rate. We assembled a structurally dissimilar collection of *Sequoia* shoots by broadly manipulating climatic factors during leaf development both within the native range and at a hotter, low rainfall location outside it. Experimental occlusion of stomata along with application of florescent tracers to leaf surfaces, allowed us to ascertain the primary uptake route. Variability of leaf structures associated with both the uptake pathway and capacity allows us to strategically isolate key traits for future investigations into the impacts of climate change on *Sequoia*'s ability to exploit leaf wetness.

Methods

Maximization of trait diversity – In order to explore foliar traits enhancing or limiting water absorption capacity, and assess their degree of responsiveness to climatic factors, we sought to maximize the diversity of leaf structure. Trait variation was induced in two ways. First, we selected two locations with small but mature *Sequoia* trees with leaves accessible from ground-level, one a natural forest in the heart of the species' northern range (private land, Humboldt County, CA, 40.8 °N, 124.0 °W), and a second hot, low-rainfall site with access to landscape irrigation, well outside the historic range of the species but at a latitude where they occur (UC Davis campus, Davis, CA, 38.5 °N, 121.7 °W, **Table 3.1**). Second, at each location we placed clear plastic bags around 20 shoots shortly after they completed their expansion (last week of April, 2020), and left them in place until their harvest at full leaf-hardening (last week of January 2021). Bagging did not appear to influence the coverage of epiphyllic organisms, which are visible in resin imprints (**Fig 3.1c**). The intention behind the bagging was to create miniature greenhouses, simultaneously altering evaporative demand, exposure, and thermal conditions during leaf development in order to induce maximum breadth of leaf phenotypic expression. Because our interest for this initial investigation was in the environmental malleability of foliar uptake, rather than identifying effects of individual climatic factors and their interactions, we focused on potential extremity of leaf structure, not its causes. With this approach, we had four classes of shoots, in-range bagged, in-range untreated, outside-range bagged, and outside-range untreated, across which to explore how uptake parameters are influenced by anatomical-structural responses to climatic conditions (**Table 3.1**).

Measurement of foliar water uptake kinetic parameters After harvesting samples from all four shoot-classes, we bench-dried samples with a collection of both bagged and un-bagged shoots (1 bag with several shoots per sample). Following 24-hr equilibration in the dark, we obtained initial water

potential (Ψ) from a shoot off each sample. Foliar water uptake was measured following the rehydration kinetics based method of Guzmán-Delgado *et al*. (2018), where a set of weighed leaves was placed in a fog chamber and removed at ~ 15-min intervals. Following removal, final weight and Ψ were measured for each individual shoot (*N* = 12-19 per class). Fresh shoots were then carefully dissected into individual leaves and scanned to obtain leaf area, before kiln-drying at 100 °C for final dry-mass. Shoot-specific "uptake" was measured in g m^{-2} min^{-1} for PCA and trait analyses.

To obtain kinetic parameters representing water absorption in each shoot-class, we plotted the three-parameter logistic relationship of water absorption (g m^{-2}) against time (minutes), resulting in 4 curves made up of individual shoot samples, one for each shoot-class (**Table 3.1**). Logistic curves were used to estimate total uptake over 5-hr and 7-hr fog-exposure periods. From the first derivative of the logistic curves, we estimated maximum uptake rate (g m^{-2} min^{-1}) and the time constant (time to maximum rate, **Table 3.1**). We calculated conductivity for each shoot-class by dividing the 7-hr uptake estimate by the initial shoot Ψ.

Measurement of leaf traits – From a sub-set of sampled branches we removed a representative bagged and control shoot (N = 6 per shoot-class, **Fig. 3.1a**). These shoots were used fresh and un-treated for the measurement of foliar traits representing individual bags or neighboring sets of control-shoots (**Table 3.2**). Stomatal density, stomatal bed width, and guard-cell length were measured from acrylic-resin imprints, surface wax coverage was obtained using color-thresholding of macro images to select wax (**Fig. 3.1b,c**). Water droplet contact angle was measured from photos of 10-µL droplets of DI water taken at 10X through a sideways microscope (**Fig 3.1d**). Epidermal traits were measured from 40X digital images of fresh green cross-sections that were cut with a microtome at a thickness of 10 µm, and mounted un-stained in water (**Fig 3.1e**, **Table 3.2**).

Determination of the foliar uptake pathway – Consideration of the traits related to water absorption into leaves requires verification of the absorption pathway. Conveniently, at ground-level it is

possible to locate shade-grown *Sequoia* shoots where the adaxial surface is free of stomata, easily verified by the presence of their large, reflective, wax plugs. To determine whether water crosses the leaf cuticle or enters via stomata, we painted each individual leaf on a shoot with melted paraffin, to occlude stomata and block the cuticle. Carefully covering only the stomata-free adaxial surface, stomata-covered abaxial surface, or both, with a layer of wax. A set of wax-free shoots were used as a control group. Shoots were weighed with the wax intact, and then suspended in a fog chamber for 3 hours before reweighing. Because small quantities of water clung to imperfections in the waxed surfaces, we subtracted one-half the mean weight-gain of shoots with 2 waxed surfaces from final weights of all those with single-waxed surfaces, as a correction factor. While a rough correction, it appeared to be reasonable as our corrected estimates of abaxial and adaxial uptake summed to a value very near that expected for the whole leaf.

To further confirm our experimental results, we applied droplets of the aqueous, exclusively apoplastic, florescent stain, Sulforhodamine B, in a concentration of 0.001 % to adaxial leaf surfaces for 1 hour while leaves remained attached to the shoot, and the shoot retained access to water. Droplets were applied to stomata-free portions of the mid-leaf. Stained leaves were thoroughly rinsed and blotted dry before immediate sectioning with a microtome using a dry blade and avoiding any exposure of the cut surface to water. Cuts were made adaxial-side down, right-to-left from one leaf corner to the other so that if any un-bound dye were carried by the blade, it would be apparent in the direction of spread. We did not observed any indication of stain spreading as a sectioning artefact. The resulting cross-sections were mounted dry and without coverslip, and photographed alongside identically-prepared, unstained leaf-sections from the same shoot 10X, 20X, and 40X under a 535 nm reflected fluorescent light source. We found that “thick” 20-µm sections provided the best compromise between drying before photography, and image clarity.

Data analysis – The effects and interactions of location and bagging on foliar water uptake were assessed with a permutation-based two-way factorial test, using 5000 runs in the R package asbio(). To avoid multiple univariate comparisons of our 15 traits to uptake, we began with a multivariate approach to explore the variation of traits among our 4 shoot-classes as they related to the phenomenon of interest, uptake (g m^{-2} min^{-1}). Using mean shoot values for each bag or sample (N = 23), Principal Components Analysis (PCA) was employed to assess the separation of the 4 shoot-classes in trait-space and the relationship of the resulting axes (Principal Components, PCs) to uptake. Starting with the complete 15-trait set, we performed an initial PCA, then removed 5 traits with the most orthogonal relationships to uptake as visualized in the biplot of trait-vectors over the first two PCs. The 10 traits retained for the second PCA round (**Table 3.2**) had a mean skewness of 0.15 and mean kurtosis of 0.93, with no individual kurtosis values > 2.1, Euclidean distance was used as a measure. To further reduce dimensionality, only the first five resulting PCs, retaining 78 % of the trait information, were used to calculate the size and position of the 5-dimensional volumes occupied by location and bagging-classes within the shared ordination space, and quantify their overlap with the R package hypervolume().

The 10 traits identified through our initial PCA were used in step-wise multiple linear regression (starting with the saturated model lacking interaction terms), to look for meaningful relationships between the traits measured and parameters representing variation in water absorption. At each step the lowest-preforming trait was removed and using AICc, R^2, and parameter error were recalculated and used as selection criteria, adding the trait back if its removal did not improve scores. Where the top model had more than one predictor, a model with interaction terms for the predictors was also examined. The individual and interactive effects of location and bagging on the three traits in our top models were assessed collectively with permutation-based factorial tests, and individually with two-sided asymptotic general independence tests in the R package coin(). The relative developmental plasticity (coefficient of variation, SD/mean) of each of the 15 traits was calculated to compare the

breadth of their responsiveness. A two-sided asymptotic general independence test was used to compare uptake of leaves with waxed adaxial surfaces to those with waxed abaxial surfaces. PCA was performed in PC-ORD 5 (McCune 1986), and all other analyses and calculations were done in R (R Core Team).

Results

Differences in foliar uptake kinetic parameters Foliar water uptake (g m^{-2} min^{-1}) of individual shoots is dependent on tree location, but not on the effects of bagging, or the interaction of location and bagging (location: F = 13.15, P-value = 0.0014; bagging: F = 0.78, P-value = 0.3914; location x bagging: F = 0.66, P-value = 0.4398). Shoots grown outside the natural range have higher uptake as a group (**Fig 3.2a**). This effect leads to substantial differences in kinetic parameters such as logistic curve shape, maximum uptake rates, time constants, and surface hydraulic conductivity among the 4 shoot-classes, such that the outside-range bagged shoots have roughly double the maximum uptake rate of the in-range untreated shoots (**Fig 3.2b**, **Table 3.1**).

Differences in leaf traits — Leaf traits differ among locations and collectively and individually respond to the broad variation in climatic stimuli captured in this study (**Table 3.1**). PCA resulted in 1 significant axis that retained 27 % of the variation in the 10 structural traits used (**Table 3.2**), helped explain uptake (N = 23, R^2 = 0.57), and revealed a distinct separation of samples based on their location (**Fig 3.2c**). The hypervolumes defined by the first 5 PCs, containing 78 % of the total variation in the 10 traits, reveal that the two locations (in and out of range) have zero spatial overlap, while bagged and control shoots occupy < 10 % of the same trait-space. The relative size of their hypervolumes suggests that native-range shoots are the most homogenous group, their relative unit-less volumes are: Bagged shoots: 11^5, Untreated shoots: 13^5, In-range: 5^5, Outside-range: 15^5.

Traits determine foliar water uptake parameters– The top two trait-based linear models for uptake both contained abaxial wax coverage and stomatal density as the predictors, both of which have a negative effect on uptake. The model with the best fit (N = 23, R^2 = 0.65, P-value = 0.0002) and lowest AICc score is the interaction of wax and stomatal density. While the model with an interaction term is ~ 50 % more likely than the next-best additive model (N = 23, R^2 = 0.55, P-value = 0.0003, **Fig 3.2d**), it has > 3X the relative error on its parameter estimates, making it a relatively poor predictor and mostly useful from a phenomenological perspective in understanding the collective importance of those two traits. The mean abaxial wax coverage in each shoot-class is the only trait useable as a predictor for shoot-class maximum uptake (N = 4, R^2 = 0.96, P-value = 0.0224). Apoplastic thickness between epidermal cell lumens appears to have a positive, non-linear effect on these kinetic parameters, suggesting that it may be worthy of further investigation, using a larger number of absorption curves.

Among the two key predictive traits identified through multivariate modeling procedures, abaxial wax coverage is strongly effected by location (F = 19.57, P-value = 0.001) but not bagging treatment or their interaction. Stomatal density is nearly, but not significantly, dependent on bagging alone (F = 3.37, P-value = 0.083, **Table 3.2**). Apoplastic thickness and abaxial wax coverage had the least developmental plasticity of the 15 traits measured in this study (**Table 3.2**).

Confirmation of the uptake pathway – Water crosses *Sequoia* leaf surfaces primarily, if not entirely, via the cuticle, not through stomata. Shoots with their stomata-covered abaxial surfaces sealed with paraffin still absorb ~ 3X the water over three hours (N = 4, mean = 0.14517 mg mm^{-2}) compared to leaves with exposed stomata and covered stomata-free adaxial surfaces (mean = 0.049054 mg mm^{-2}, Z = 2.8284, P-value = 0.0047). The sum of the mean single-side uptake values (N = 5, 0.1942 mg mm^{-2}) is nearly equal to the mean uptake of un-waxed control leaves (N = 5, 0.2071 mg mm^{-2}). Interestingly, quantity of water absorbed through the abaxial surface, ~ 25 % of uptake, does not correspond to the generally low-wax, spaces between the two stomatal beds and along leaf edges which collectively cover

almost half of the surface (**Fig 3.1b**). Additionally, after 1-hr of adaxial-surface exposure to Sulforhodamine B, which cannot cross membranes, the stain is visible inside the leaf (**Fig. 3.3a**). Patterns of dye visibility suggest that post-absorption hydraulic transport is both apoplastic and symplastic. A hydraulic path can be traced through the apoplast, from the epidermal site of dye application, directly to the vascular tissue (**Fig. 3.3b**). At the same time, bright areas of dye concentration in external epidermal and hypodermal walls, indicate that a portion of the water absorbed by leaves enters the symplast at those points, leaving the Sulforhodamine it carries to accumulate outside the cellular membrane (**Fig. 3.3c**).

Discussion

Developmental responsiveness of leaf-traits to micro-climatic conditions shapes foliar water uptake capacity in *Sequoia* by altering patterns of absorption though the cuticle. In an exciting verification, the key traits associated with uptake variation in our broad trait evaluation, abaxial wax coverage and stomatal density, have been previously implicated as causes of hydraulic resistance at the leaf surface using other approaches (Chin *et al.* in prep). These two traits have relatively high developmental plasticity (**Table 3.2**), and their collective effects contribute to the large differences in uptake parameters associated with location and treatment (**Fig. 3.2**). Negative effects of stomatal density on water absorption corroborate a lack of stomatal involvement in the transcuticular water-entry route we confirm for *Sequoia.* As observed in some angiosperm species (Eller *et al.* 2013, Boanares *et al.* 2018), the path of water carrying a fluorescent tracer can be seen passing the cuticle in stomata-free portions of the leaf surface (**Fig. 3.3a**). Additionally, experimental occlusion of stomata does not prevent foliar water uptake in *Sequoia*, nor suggest that vapor passing through open stomata makes notable contributions to otherwise cuticular water absorption in this particular species (Guzmán-Delgado *et al.* 2021). There is a distinct apoplastic pathway leading from the surface to the vascular

tissue (**Fig. 3.3b**), however an unquantified portion of absorbed water appears to enter the symplast of epidermal and hypodermal cells (**Fig. 3.3c**). Unlike *Picea glauca*, where aquaporin upregulation under condensation-conditions implies symplastic water transport (Laur & Hack 2014), *Sequoia* lacks a suberized endodermis that forces water to cross a membrane before reaching the vein − making fully apoplastic transport possible and hinting at family-level differences in conifer hydraulic pathways outside the vascular cylinder. The weak relationship we observed between uptake rate and apoplastic tension, as measured with a pressure chamber (R^2 = 0.26, N = 63), seemingly contradicts a primarily apoplastic hydraulic path. However, potential changes in apoplastic osmotic concentration during the course of water absorption (not measure here) could help explain this surprising lack of correlation.

Cuticular thickness, wettability, and other leaf attributes that respond to environmental variation without meaningfully influencing uptake capacity in *Sequoia*, are equally informative (**Table 3.2**). Lack of influence of cuticular thickness on uptake − despite a cuticular uptake route − implies that resistance contributed by this portion of the hydraulic pathway is swamped by processes occurring at the leaf surface. In *Sequoia*, a thick cuticle seems, if anything, to be associated with high uptake rates, this may be related to compensatory effects of increased permeability of the cuticle at high temperatures (Riederer & Schreiber 2001), as seen in our outside-range location or the association of cuticular thickness with humidity (Berlyn *et al.* 1993), which was likely higher in bags. Passage across the cuticle fits with observations of flavonol autofluorescence in *Sequoia*'s cuticle (Chin, unpublished data), flavonols are polar molecules, which may create a diffusive pathway for hydraulic entry into the leaf (Riederer & Schreiber 2001, Schreiber 2005). Interestingly, the least wettable surfaces were associated with bagged outside-range samples, which had the highest maximum uptake rate (**Fig. 3.2b**). While surface resistance can be largely attributed to wax coverage, it is apparently not related to wettability as in some species (Neinhuis & Barthlott 1997, Koch *et al.* 2006), thus we wonder if the mechanism by which wax causes hydraulic resistance might involve increasing the distance between droplets and the

leaf surface (Bhushan & Jung 2008), rather than preventing droplet spread. Surface waxes may have the potential to be especially responsive to climatic variation because they are one of the few attributes of leaves that can change even in age (Baker 1974). Our results are an interesting contrast to the association of surface waxes with low humidity and high temperature (Koch *et al.* 2006). Regardless, geographic variation in wettability and water absorption, as observed here, suggests possibly important regional differences in forest capacity for interception and retention of rainfall and fog (Azevedo & Morgan 1974, Holder 2007, Konrad *et al.* 2012).

Potential ecological impacts of altered surface properties can be seen in the striking differences in maximum uptake rate and time constant seen between in-range and outside-range *Sequoia* shoots (**Fig. 3.2**, **Table 3.1**). Shoots grown at the hotter, low-rainfall site outside the species' native range have higher peak uptake rates and reach their maximum uptake in ~ 2.5 hours, approximately double the rate, reached twice as fast, as un-manipulated shoots grown in the wet northern range (**Fig. 3.2, Table 3.1**). We speculate that frequent leaf-wetting promotes the development of surface waxes as an acclimation to avoid limitation of gas exchange by water on the stomatal beds (Chin Chapter 2). Interestingly, while bagging did not change the time constant in outside-range samples, it moved in-range kinetic parameters closer to the outside-range values (**Fig. 3.2**, **Table 3.1**). We had presumed that bagging would have a multi-factor greenhouse-like effect, however it is worth considering that excluding natural leaf-wetting events in the wet native range may have acclimated leaves for low-wetness environments. Where leaf wetting events are scare, benefits of enhanced uptake may outweigh infrequent costs of water-limited stomatal conductance. The availability of soil-water at both sites suggests that frequent leaf wetness, rather than plant water-status, promotes leaf traits that increase surface hydraulic resistance by reducing water-contact with the absorbent cuticle. Due to differences in conductivity and maximum rate we expect that in attached shoots, where whole-tree Ψ would remain relatively low, outside-range shoots can absorb more water over any length leaf-wetting event (**Table**

3.1). The higher conductivity of outside-range shoots indicates that they are better able to exploit brief leaf-wetting events, and that a larger portion of intercepted water would be absorbed rather than dripped to the soil or evaporated from the leaf surface.

As this study was focused on traits and assessment of *Sequoia*'s developmental repertoire under wide-ranging climatic variation, we made no attempt to evaluate the impacts of individual climatic factors. While this is not without value, the effects of individual or small groups of environmental parameters are difficult to interpret in the multi-factor context of site suitability, range limitation, or climate change, and do not inform us about change in the forest. Rather, we encourage future *Sequoia* researchers and forestation practitioners to consider and explore the two key traits identified here on a regional and genomic basis, particularly along dry eastern and southern range margins. As relatively macroscopic features of leaf surfaces, wax coverage and stomatal density are particularly usefully traits for ecological monitoring. Ease and low cost of measurement mark these two crucial features as highly suitable for large scale projects, including those involving volunteers with limited training, thus opening the potential for citizen-science. Low developmental stability further suggests the utility of surface wax and stomata for comparison across *Sequoia*'s geographic range and for long-term monitoring.

Shoot behavior demonstrates surprisingly broad bagging-associated alteration of foliar water uptake parameters (**Fig. 3.2a,b**). Acclimation of traits controlling uptake within a single growing season (**Table 3.2**, **Fig. 3.2d**), including probable regional differences in the ability to utilize short-duration leaf-wetting events (**Table 3.1**), indicates that interactions of *Sequoia* forests with atmospheric water are essentially unstable, having the potential to change dramatically with climatic perturbation. Isotopes indicate interception by *Sequoia* trees almost doubles the annual hydrologic contributions of fog drip to the system, and although > 40 years ago, up to 40 cm of fog drip has been collected in *Sequoia* forests during summer (Azevado & Morgan 1974, Dawson 1998). We expect that, like uptake, these hydrologically important levels of fog drip are also influenced by waxiness and stomatal density of

Sequoia leaves or by other surface factors, such as wettability, where we observed climate-induced developmental plasticity (**Table 3.2**). Like the majority of plants in *Sequoia* forests, exploitation of leaf wetness makes critical contributions to plant dry-season survival and ecosystem water cycling worldwide (Breshears *et al.* 2008, Limm *et al.* 2009, Eller et al. 2016, Emery 2016, Gotsch *et al.* 2016, Binks *et al.* 2019). While we expect that the surface traits controlling uptake will have phylogenic specificity, detection of similar attributes (eg. hydroids: Gotsch *et al.* 2016, trichomes: Ohrui *et al.* 2007 & Fernández *et al.* 2014) in other system-dominating taxa is needed before we can explore their change over time and connect developmental expression to ecological patterns. Isolating key functional traits can be a first step in a conservation-physiology (Seebacher & Franklin 2012) approach to establishing mechanistic and causative links between climate, trait plasticity, and ecosystem responsiveness to global change.

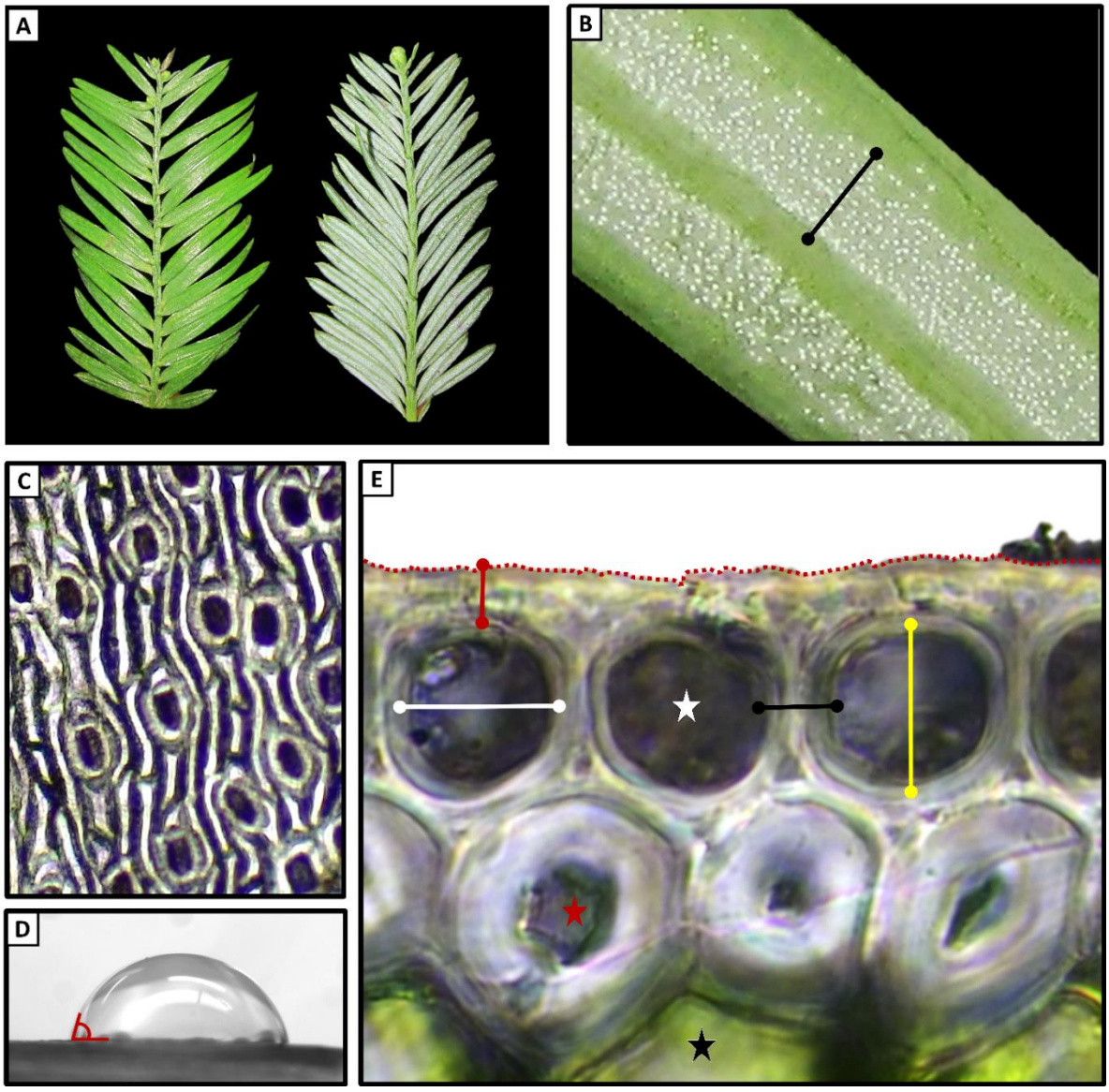

Figure 3.1. Traits of *Sequoia sempervirens* leaf surfaces and their measurement. A) The adaxial surface (left) lacks the visible waxes of the abaxial surface (right). **B**) Stomata on the abaxial surface, visible as white dots, occur in 2 beds on either side of the vein, Black spanner = bed width. **C**) Stomatal density and guard cell length were measured from resin imprints. **D**) Contact angles of water droplets with the leaf surfaces were used to indicate wettability. **E**) Cross-section through the adaxial epidermis (40X). White star = epidermal cell, red star = hypodermal cell, black star = mesophyll cell. Dotted red line = surface pathlength used to measure rugosity. Red spanner = cuticle thickness, white spanner= epidermal lumen width, yellow spanner = epidermal lumen height, black spanner = apoplastic thickness. See written descriptions in Table 2.

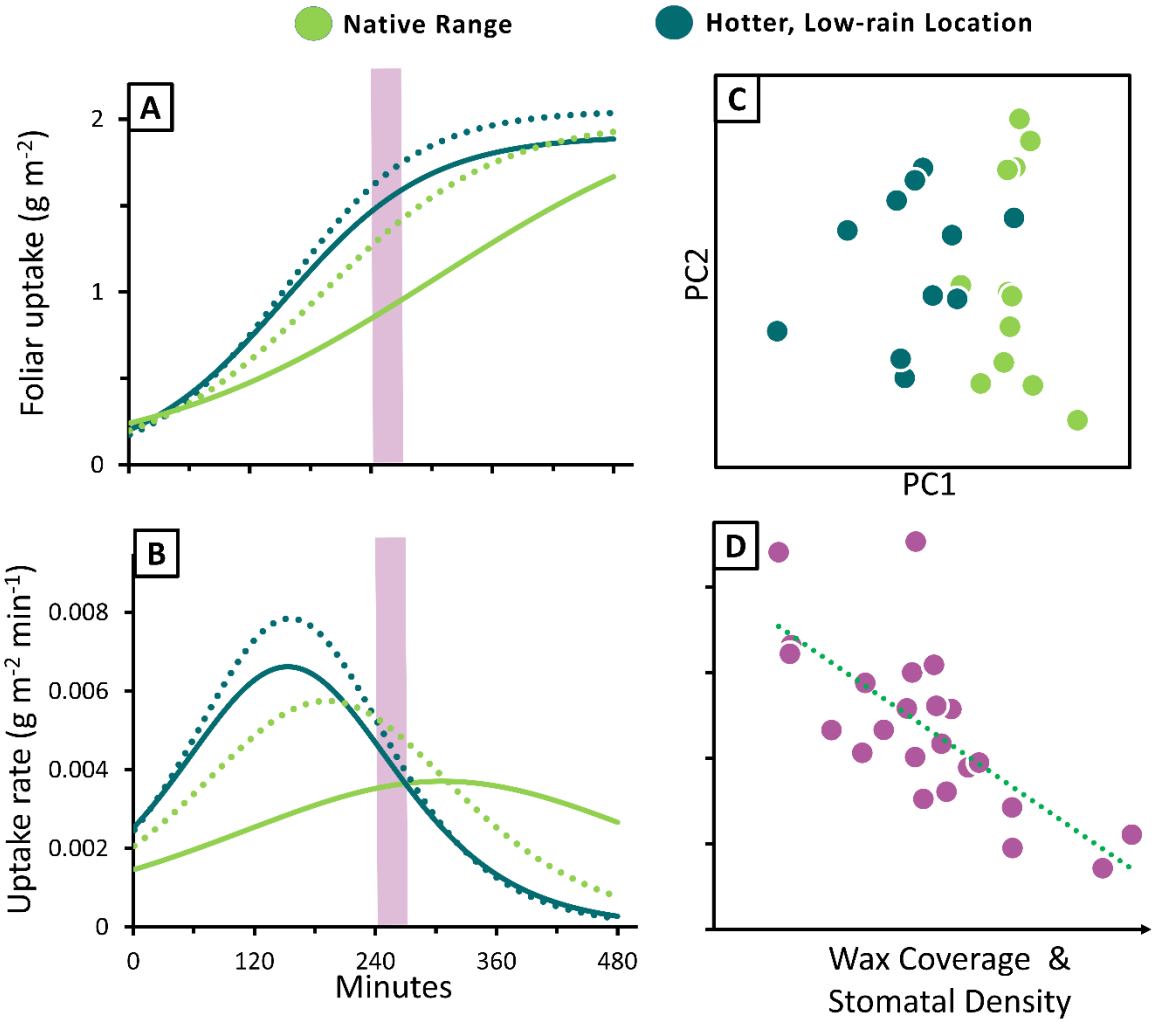

Figure 3.2. Climate alters leaf uptake capacity and structure. A and B) Logistic foliar uptake curves (**A**) for each of our 4 treatment classes, and their first derivative showing change in rate over time (**B**), dotted lines indicated bagged samples. Purple bars highlight the time point after which uptake rate is higher in samples grown at the native-range location, but where location-difference in cumulative uptake is greatest. **C**) Principal components analysis of 10 leaf traits shows a clear separation of shoots by location in the first axis (PC1), which is negatively associated with uptake R^2 = 0.57. **D**) The relationship between uptake rate (g m^{-2} min^{-1}) and the interaction of abaxial wax coverage and stomatal density R^2 = 0.65. Shoots with a combination of high wax and high stomatal density have the slowest uptake.

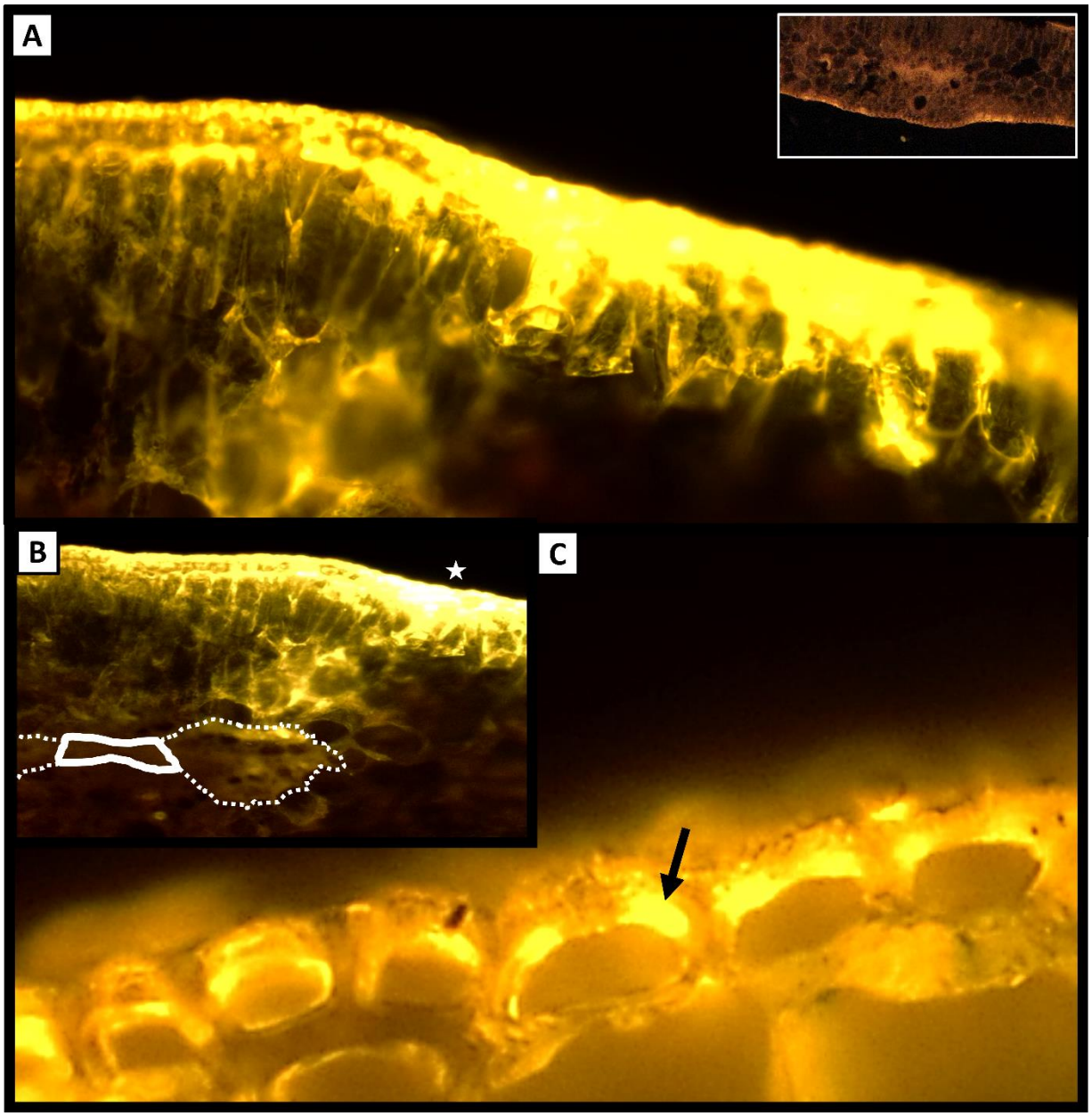

Figure 3.3. Water enters *Sequoia sempervirens* leaves via the cuticle. **A**) The path of water carrying the fluorescent yellow tracer Sulforhodamine B can be seen traversing a stomata-free region of the adaxial surface. 20X. Inset in upper right corner shows the natural orange autofluorescence of unstained leaves at the same wavelength (535 nm). Autofluorescence is nearly invisible at the low brightness used to photograph the stain. **B**) The visibility of dye in the mesophyll and vein conclusively demonstrates an apoplastic pathway from the adaxial site of water application (star) to the vascular tissue (dotted lines = transfusion tissue, white line = xylem). 10X. **C**) Accumulation of dye external to lumens of epidermal cells (bright spots as at arrow) suggests that a portion of absorbed water might enter the symplast at these points, leaving stain outside the cellular membrane. Yellow "haze" is an artefact of stain fluorescence from the sides of the thick section 40X.

Table 3.1. Treatments on *Sequoia sempervirens* shoots and their resulting uptake parameters. Temperature and rainfall reflect locational differences during our May 2020-January 2021 study period (PRISM 2021). For logistic models of the relationship between g m^{-2} and time, RMSE can be compared to the asymptote to understand model error. Estimated uptake for 5 and 7-hr periods are the predicted total for that timespan from the logistic curves. Maximum rate is the peak value of the first derivative of the logistic curve, and the time constant is the minutes of fog exposure before the maximum rate is attained. Conductivity is calculated by dividing the 7-hr estimated uptake by initial water potential before fog exposure.

					Normalized Mean (0,1)			
					In-Range		Outside-Range	
Trait	Definition	Units	Grand Mean	Plasticity (%)	Untreated	Bagged	Untreated	Bagged
Apoplastic thickness*	Thickness of the apoplastic space between adaxial epidermal cell lumens	mm	0.0069	32	0.23	0.26	0.33	0.60
Abaxial wax coverage*	Covering fraction of visible waxes on the abaxial surface	–	0.53503	23	0.72	0.57	0.38	0.28
Hypodermal thickness	Thickness of adaxial hypodermal cells	mm	0.0262	22	0.45	0.58	0.70	0.50
Stomatal covering fraction	Guard-cell length per area, an index of total pore coverage	mm mm^{-2}	3.6661	22	0.37	0.61	0.49	0.67
Epidermal cell lumen height*	Internal height of adaxial epidermal cell lumens	mm	0.0109	21	0.48	0.68	0.51	0.40
Stomatal bed width*	Width of abaxial stomatal beds	mm	0.5854	21	0.33	0.18	0.54	0.55
LMA*	Leaf dry mass per fresh area	g m^{-2}	10.07961	20	0.66	0.62	0.79	0.73
Stomatal density*	Number of stomata per area on the abaxial surface	count mm^{-2}	112	20	0.37	0.56	0.39	0.58
Adaxial wettability	Water droplet contact angle to leaf adaxial surface, smaller angles indicate greater wettability	angle	65.3	20	0.16	0.46	0.19	0.54
Cuticle thickness*	Distance between adaxial epidermal cell walls and the leaf surface	mm	0.0070	18	0.33	0.51	0.34	0.60
Epidermal cell lumen width*	Internal width of adaxial epidermal cell lumens	mm	0.0144	16	0.62	0.71	0.43	0.49
Stomatal bed fraction	Fraction of the abaxial leaf surface occupied by stomatal beds	–	0.53	15	0.48	0.43	0.34	0.42
Stomatal guard cell length*	An index of maximum stomatal apperature	mm	0.0328	14	0.46	0.54	0.61	0.58
Abaxial wettability	Water droplet contact angle to leaf abaxial surface, smaller angles indicate greater wettability	angle	89.4	10	0.41	0.76	0.53	0.80
Surface rugosity*	Linear distance per adaxial surface pathlength, smaller numbers indicate rougher surfaces	–	0.9813	2	0.71	0.86	0.72	0.60

Table 3.2. Traits of *Sequoia sempervirens* leaf surfaces and their developmental plasticity. The 10 traits with * were used in PCA and multiple regression. CV is the coefficient of variation (SD/mean expressed as a percent), used here as an index of trait developmental plasticity across all treatments. Treatment means are normalized by the full range of observed values for purposes of comparison. Traits ordered by plasticity, see visual depictions of trait measurements in **Figure 1**.

Treatment	Maximum Temperature (°C)	Rainfall (mm)	N	Logistic Model Asymptote	RMSE	5-hr Estimated Uptake ($g\ m^{-2}$)	7-hr Estimated Uptake ($g\ m^{-2}$)	Maximum Uptake Rate ($g\ m^{-2}\ min^{-1}$)	Time Constant (min)	7-hr Mean Conductivity ($g\ m^{-2}\ min^{-1}\ MPa^{-1}$)
In-Range Untreated	26.4	701	15	2.181	0.4267	1.0689	1.4938	0.00370	306	0.00156
In-Range Bagged			17	1.998	0.5198	1.5535	1.8643	0.00575	191	0.00190
Outside-Range Untreated	35.4	126	19	1.906	0.4703	1.6881	1.8604	0.00662	153	0.00206
Outside-Range Bagged			12	2.052	0.4185	1.8509	2.0168	0.00785	154	0.00235

Literature Cited in Chapter 3

Azevedo, J. and Morgan, D.L., 1974. Fog precipitation in coastal California forests. Ecology, 55:1135-1141.

Baker, E.A., 1974. The influence of environment on leaf wax development in Brassica oleracea var. gemmifera. New Phytologist, 73:955-966.

Barthlott, W. and Neinhuis, C., 1997. Purity of the sacred lotus, or escape from contamination in biological surfaces. Planta, 202:1-8.

Berlyn, G.P., Anoruo, A.O., Vann, D.R., Johnson, A.H., Strimbeck, G.R., Boyce, R.L. and Silver, W.L., 1993. Effects of filtered air and misting treatments on cuticles of red spruce needles on Whiteface Mountain, NY. Journal of Sustainable Forestry, 1:25-47.

Berry, Z.C., Emery, N.C., Gotsch, S.G. and Goldsmith, G.R., 2019. Foliar water uptake: processes, pathways, and integration into plant water budgets. Plant, cell & environment, 42:410-423.

Bhushan, B. and Jung, Y.C., 2008. Wetting, adhesion and friction of superhydrophobic and hydrophilic leaves and fabricated micro/nanopatterned surfaces. Journal of Physics: Condensed Matter, 20:225010.

Binks, O., Mencuccini, M., Rowland, L., da Costa, A.C., de Carvalho, C.J.R., Bittencourt, P., Eller, C., Teodoro, G.S., Carvalho, E.J.M., Soza, A. and Ferreira, L., 2019. Foliar water uptake in Amazonian trees: Evidence and consequences. Global change biology, 25:2678-2690.

Boanares, D., Isaias, R.R.M.S., de Sousa, H.C. and Kozovits, A.R., 2018. Strategies of leaf water uptake based on anatomical traits. Plant Biology, 20:848-856.

Burgess, S.S.O. and Dawson, T.E., 2004. The contribution of fog to the water relations of Sequoia sempervirens (D. Don): foliar uptake and prevention of dehydration. Plant, Cell & Environment, 27:1023-1034.

Chin, A.R. and Sillett, S.C., 2019. Within-crown plasticity in leaf traits among the tallest conifers. American Journal of Botany, 106:174-186.

Dawson, T.E., 1998. Fog in the California redwood forest: ecosystem inputs and use by plants. Oecologia, 117:476-485.

Dawson, T.E. and Goldsmith, G.R., 2018. The value of wet leaves. New Phytologist, 219:1156-1169.

Eller, C.B., Lima, A.L. and Oliveira, R.S., 2013. Foliar uptake of fog water and transport belowground alleviates drought effects in the cloud forest tree species, Drimys brasiliensis (Winteraceae). New Phytologist, 199:151-162.

Eller, C.B., Lima, A.L. and Oliveira, R.S., 2016. Cloud forest trees with higher foliar water uptake capacity and anisohydric behavior are more vulnerable to drought and climate change. New Phytologist, 211:489-501.

Emery, N.C., 2016. Foliar uptake of fog in coastal California shrub species. Oecologia, 182:731-742.

Fernández, V., Sancho-Knapik, D., Guzmán, P., Peguero-Pina, J.J., Gil, L., Karabourniotis, G., Khayet, M., Fasseas, C., Heredia-Guerrero, J.A., Heredia, A. and Gil-Pelegrín, E., 2014. Wettability, polarity, and water absorption of holm oak leaves: effect of leaf side and age. Plant Physiology, 166:168-180.

González, A. and Ayerbe, L., 2010. Effect of terminal water stress on leaf epicuticular wax load, residual transpiration and grain yield in barley. Euphytica, 172:341-349.

Gotsch, S.G., Nadkarni, N., Darby, A., Glunk, A., Dix, M., Davidson, K. and Dawson, T.E., 2015. Life in the treetops: ecophysiological strategies of canopy epiphytes in a tropical montane cloud forest. Ecological Monographs, 85:393-412.

Guzmán-Delgado, P., Mason Earles, J. and Zwieniecki, M.A., 2018. Insight into the physiological role of water absorption via the leaf surface from a rehydration kinetics perspective. Plant, Cell & Environment, 41:1886-1894.

Guzmán-Delgado, P., Laca, E. and Zwieniecki, M.A., 2021. Unraveling foliar water uptake pathways: the contribution of stomata and the cuticle. Plant, Cell & Environment.

Holder, C.D., 2007. Leaf water repellency of species in Guatemala and Colorado (USA) and its significance to forest hydrology studies. Journal of Hydrology, 336:147-154

Kerstiens, G., 2006. Water transport in plant cuticles: an update. Journal of experimental botany, 57:2493-2499.

Koch, K., Hartmann, K.D., Schreiber, L., Barthlott, W. and Neinhuis, C., 2006. Influences of air humidity during the cultivation of plants on wax chemical composition, morphology and leaf surface wettability. Environmental and Experimental Botany, 56:1-9.

Konrad, W., Ebner, M., Traiser, C. and Roth-Nebelsick, A., 2012. Leaf surface wettability and implications for drop shedding and evaporation from forest canopies. Pure and Applied Geophysics, 169:835-845.

Laur, J. and Hacke, U.G., 2014. Exploring Picea glauca aquaporins in the context of needle water uptake and xylem refilling. New Phytologist, 203:388-400.

Limm, E.B., Simonin, K.A., Bothman, A.G. and Dawson, T.E., 2009. Foliar water uptake: a common water acquisition strategy for plants of the redwood forest. Oecologia, 161:449-459.

Limm, E.B. and Dawson, T.E., 2010. Polystichum munitum (Dryopteridaceae) varies geographically in its capacity to absorb fog water by foliar uptake within the redwood forest ecosystem. American Journal of Botany, 97:1121-1128.

McCune, B., 1986. PC-ORD: an integrated system for multivariate analysis of ecological data. Abstracta Botanica, pp.221-225.

Neinhuis, C. and Barthlott, W., 1997. Characterization and distribution of water-repellent, self-cleaning plant surfaces. Annals of botany, 79:667-677.

Ohrui, T., Nobira, H., Sakata, Y., Taji, T., Yamamoto, C., Nishida, K., Yamakawa, T., Sasuga, Y., Yaguchi, Y., Takenaga, H. and Tanaka, S., 2007. Foliar trichome-and aquaporin-aided water uptake in a drought-resistant epiphyte Tillandsia ionantha Planchon. Planta, 227:47-56.

Riederer, M. and Schreiber, L., 2001. Protecting against water loss: analysis of the barrier properties of plant cuticles. Journal of experimental botany, 52:2023-2032.

Rundel, P.W., 1982. Water uptake by organs other than roots. In Physiological plant ecology II (pp. 111-134). Springer, Berlin, Heidelberg.

Schreel, J.D. and Steppe, K., 2020. Foliar water uptake in trees: negligible or necessary?. Trends in Plant Science.

Schreiber, L., 2005. Polar paths of diffusion across plant cuticles: new evidence for an old hypothesis. Annals of Botany, 95:1069-1073.

Seebacher, F. and Franklin, C.E., 2012. Determining environmental causes of biological effects: the need for a mechanistic physiological dimension in conservation biology. Philosophical Transactions of the Royal Society B: Biological Sciences, 367:1607-1614.

Simonin, K.A., Santiago, L.S. and Dawson, T.E., 2009. Fog interception by Sequoia sempervirens (D. Don) crowns decouples physiology from soil water deficit. Plant, Cell & Environment, 32:882-892.

Sultan, S.E., 2017. Developmental plasticity: re-conceiving the genotype. Interface Focus, 7:201700

Dissertation Acknowledgements

I am truly grateful to my Major Professor M. Zwieniecki for guiding me to become a better, more independent scientist and inspiring me to consider what I can calculate, instead of just what I can measure. I was also helped and encouraged throughout by P. Guzmán Delgado and S. Sillett, both excellent colleagues and wonderful friends, I can't thank them enough for being there for me. I greatly benefited from the kind help of my committee members A. McElrone, H. Safford, and T. Young, as well as collaboration with, L. Kerhoulas, J. Orozco, J. Godfrey, A. Amico Roxas, Z. Moore, R. Kramer, A. Ambrose, and M. Reed. I also wish to thank D. Parkinson and H. Barnard at the Advanced Light Source for their assistance, and R. Van Pelt for providing the tree illustration in Figure 1.2. I was generously supported by a Graduate Research Fellowship from NSF, and a fellowship from the Department of Plant Sciences at UC Davis. Most of all, I thank my spouse B. Chin for support, encouragement, and assistance at every step.